bioRxiv preprint doi: https://doi.org/10.1101/667519; this version posted June 11, 2019. The copyright holder for this preprint (which was not certified by peer review) is the author/funder. All rights reserved. No reuse allowed without permission.

Sensory neurogenesis depends on vascular-neuronal filopodia contacts and blood flow

Laura Taberner[1], Aitor Bañón[1] and Berta Alsina[1]*

Developmental Biology Unit, Department of Experimental and Health Sciences, Universitat Pompeu Fabra-Parc de Recerca Biomèdica de Barcelona, Dr. Aiguader 88, Barcelona, Spain

*Author for correspondence, berta.alsina@upf.edu

bioRxiv preprint doi: https://doi.org/10.1101/667519; this version posted June 11, 2019. The copyright holder for this preprint (which was not certified by peer review) is the author/funder. All rights reserved. No reuse allowed without permission.

Summary

Cranial sensory neurons develop in close proximity to blood vessels, however neurovascular interactions in the peripheral nervous system and their underlying signals are yet unknown. Here, we uncover two separate, novel roles for cranial vasculature in cranial sensory neurogenesis in zebrafish. The first involves precise spatiotemporal endothelial-neuroblast filopodial contacts and Dll4-Notch signaling to restrain neuroblast proliferation. Secondly, we find a role for signaling triggered by blood flow in promoting sensory neuron differentiation. Thus, we demonstrate that the cranial vasculature constitutes a hitherto unrecognized signaling component of the sensory ganglia niche and controls the pace of their growth and differentiation dynamics.

Introduction

In the adult brain, neural stem cells (NSC) reside in specialized microenvironments, referred as "niches" [1,2]. There, NSCs remain relatively quiescent, but physiological or pathological circumstances can activate neurogenesis[3]. A key component in adult brain neurogenic niches is vasculature, which regulates several aspects of NSC behaviour[4–7]. In particular, two types of neurovascular interactions take place, one mediated by direct cell-cell contacts through NSC endfeet enwrapping endothelial cells (EC)[7] and the other mediated by secreted signals from EC. Cell-cell contact signaling by EphrinB2 and Jagged1 expressed in ECs and Eph and Notch receptors in NSCs regulates NSC quiescence[8]. On the other hand, endothelia secrete VEGFs, Angiopoietins, BDNF, NT-3 and PEDF that control NSC self-renewal, progenitor cell proliferation or differentiation[9–14]. During embryonic central nervous system (CNS) development, vascular and neuronal development are also tightly coupled. In the developing mouse hindbrain and telencephalon, vasculature is required for radial glia and neural/glial progenitor cell proliferation[15,16], while vasculature promotes NSC differentiation in the mouse cerebral cortex[17]. However, despite knowledge of neurovascular interactions in the CNS, there is little evidence for neurovascular crosstalk in the peripheral nervous system (PNS) during embryogenesis or adulthood.

The cranial PNS consists of several ganglia with sensory bipolar neurons that transmit external sensory information to the brain. Sensory neurons derive from neuronal precursors that are specified by *neurogenin1* (*neurog1*) in cranial sensory placodes[18]. These neuronal precursors (neuroblasts) subsequently express Neurod, delaminate and coalesce into cranial ganglia where they undergo rounds of transit-amplification and differentiate into Islet2^{+} post-mitotic sensory neurons[19–21] (Fig. 1a). Some of the autocrine signals regulating the balance between

bioRxiv preprint doi: https://doi.org/10.1101/667519; this version posted June 11, 2019. The copyright holder for this preprint (which was not certified by peer review) is the author/funder. All rights reserved. No reuse allowed without permission.

sensory neuroblast proliferation and differentiation have been described[22–27]. Since cranial blood vessels lie in close proximity to forming cranial ganglia it seems likely that vascular signals also influence their development[28]. However, this question has yet not been addressed.

In this study, we identify two novel roles for vasculature in cranial sensory neurogenesis. *In vivo* imaging of the developing sensory ganglia reveals that endothelial cells and neuroblasts establish direct contacts through filopodia. Genetic and pharmacological perturbations show that early filopodial contacts and Dll4 signaling inhibit neuroblast cell cycle entry. Later, blood flow initiation triggers cranial ganglia neuronal differentiation. Our results uncover, for the first time, that the cranial vasculature is an essential component of the sensory ganglia niche that regulates neuroblast proliferation and differentiation.

Results

Vasculature regulates the number of SAG neuroblasts through negative control of neuroblast cell cycle entry

We focused on neurovascular interactions in the statoacoustic ganglion (SAG), which forms the sensory neurons that innervate mechanosensory hair cells of the inner ear and the brainstem. The developing zebrafish SAG lies between three main vessels, the Primordial Hindbrain Channel (PHBC) that runs between the hindbrain and the otic vesicle (OV), the Lateral Dorsal Aorta (LDA) beneath the OV and the Primary Head Sinus (PHS) surrounding laterally the OV[28] (Fig. 1b).

To functionally evaluate if cranial vasculature regulates the development of cranial sensory neurons in SAG, we analyzed SAG growth dynamics in *cloche* (*clo*) homozygous mutants in the double *TgBAC(neurod:EGFP)* ^{nl1}*;(Kdrl:ras-mCherry)* ^{s896} background, in which eGFP marks sensory neurons and mCherry marks ECs. *Cloche* encodes *npas4l*, a PAS-domain-containing bHLH transcription factor required for the formation of endothelial and hematopoietic cells[29,30] and *clo* mutants have extensively been used as an avascular model[31,32]. In *clo* mutant embryos, the SAG appeared larger compared to siblings (sib) at 36 and 72 hpf (Fig. 1c). Quantification of SAG volumes revealed a statistically significant increase in *clo* mutant embryos (Fig. 1d). Moreover, the SAG displayed an abnormal shape and a significant expansion along its mediolateral axis (Fig. 1c,e). The increased volume in *clo* mutant embryos could reflect a loss of confinement of the SAG cells by taking the space left by the lack of blood vessels or, alternatively, a higher number of Neurod^{+} cells. To distinguish between both possibilities, we quantified in serial transverse sections the nuclei within the GFP-labelled SAG

bioRxiv preprint doi: https://doi.org/10.1101/667519; this version posted June 11, 2019. The copyright holder for this preprint (which was not certified by peer review) is the author/funder. All rights reserved. No reuse allowed without permission.

cells between 30 to 72 hpf in the *clo* mutant and sibling embryos (Fig. 1f and Supplementary Fig. 1). In siblings, there is a period of steep SAG growth between 30 to 36 hpf, (sib 30 hpf: 89 ± 5; sib 36 hpf: 128 ± 5). From 36 to 72 hpf, the mean number of Neurod^{+} cells is 105 ± 8, suggesting that after 36 hpf this population does not grow. Remarkably, we found that the number of Neurod^{+} cells was significantly higher in *clo* mutant embryos compared to siblings at 36 hpf (sib: 128 ± 5 vs *clo*$^{-/-}$: 177 ± 5) and this increase persisted at all the following timepoints (Fig. 1f). Several mechanisms could account for the increased number of Neurod^{+} cells in *clo* mutant embryos: i) increased specification of *neurog1*$^{+}$ cells within the otic epithelium and thereby increased delamination of Neurod^{+} cells, ii) reduced differentiation of Neurod^{+} cells into Islet2^{+} neurons or iii) increased proliferation of the transit-amplifying Neurod^{+} population. We did not find a higher number of *neurog1*$^{+}$-expressing cells in the otic epithelium in *clo* mutant embryos compared to siblings (Fig. 1g,g') nor significant differences in the number of differentiated Islet2^{+} cells in the SAG (Fig. 1h, h'). Instead, in *clo* mutant embryos we detected a significantly higher number of proliferating Neurod^{+} cells after a BrdU pulse from 24 to 30 hpf (expressed as BrdU^{+}/Neurod^{+} ratio) (Fig. 1i,i').

Thus, our results show that at early timepoints, cranial vasculature regulates the number of SAG neuroblasts by negatively controlling cell proliferation of Neurod^{+} cells and therefore constitutes an essential component of the neurosensory niche during development.

Cranial blood vessels and sensory neuroblasts establish direct contacts through filopodia

In both the embryonic and adult brain, NSCs establish contacts with ECs through endfeet projections[7,8,15]. Therefore, we wondered if neuroblasts from the SAG also establish direct contacts with the adjacent vessels. To investigate this in detail, we live-imaged sensory neuroblasts from the SAG and ECs from the PHBC in double *TgBAC(neurod:EGFP)*^{nl1}*;(Kdrl:ras-mCherry)*^{s896} reporter lines, at high spatiotemporal resolution. At 30 hpf, we did not observe neuronal extensions enwrapping ECs of the PHBC, but instead observed dynamic, thin filopodia extending from ECs to Neurod^{+} cells, as well as similar filopodia from Neurod^{+} cells extending to ECs (Fig. 2a,b, Supplementary Fig. 2, Supplementary Fig. 3 and Supplementary Video 1-4). The dynamics of filopodia were varied; in some instances, we observed filopodia extending and retracting in seconds (Fig. 2a,b cyan and magenta arrowheads respectively), in others, filopodia remained for several minutes (Fig. 2a,b, yellow arrowheads). Interestingly, some PHBC filopodia did not remain at the surface of the SAG but contacted deeper neuroblast somas (Supplementary Video 4). Moreover, stable filopodia-filopodia contacts between neuroblasts and ECs were also seen in some instances (Fig. 2c, Supplementary Fig.

bioRxiv preprint doi: https://doi.org/10.1101/667519; this version posted June 11, 2019. The copyright holder for this preprint (which was not certified by peer review) is the author/funder. All rights reserved. No reuse allowed without permission.

3). As observed in transverse optical confocal reconstructions of the vessels and the SAG, filopodia were highly directional: PHBC filopodia extended only ventrally in the direction of sensory Neurod^{+} cells (Fig. 2d,e). Interestingly, filopodia were present from 24 to 36 hpf but not later, suggesting an early role of filopodia in vessel-neuroblast communication (Fig. 2f). Altogether, highly directed and temporally regulated filopodia-mediated cell contacts are established between both EC and sensory neuroblasts.

Sensory neurons are not required for cranial vascular patterning

Communication between neurons and vessels in the CNS can take place from vessels to neurons, vice-versa and bidirectionally[33–35]. Thus, we next investigated if sensory neuron development has a role in vascular patterning near sensory ganglia. In this case, we analyzed homozygous *neurog1*^{hi1059} mutant embryos – which fail to specify sensory neuronal precursors[18]- in the double transgenic *TgBAC(neurod:EGFP)* ^{nl1}*;(Kdrl:ras-mCherry)* ^{s896} reporter line. Strikingly, despite the total absence of SAG and other cranial ganglia in *neurog1* mutant embryos, development of the PHBC and LDA displayed no obvious patterning defects at 30 hpf (Fig. 3a). The central arteries (CtAs) ingrowth into the hindbrain also did not display any delay nor obvious alteration at 48 hpf (Fig. 3a). We quantified the width of PHBC and the number of ECs at 48 hpf, and again found no significant differences between *neurog1* mutants and siblings (Fig. 3b,c). In conclusion, our data indicate that cranial vascular development does not require signals from sensory neuroblasts and suggest that primarily the signaling direction goes from vessels to neurons.

Since imaging revealed directed filopodial contacts from cranial vessels to sensory neurons and vice-versa (Fig. 2a), we wondered about possible growth interdependency. We imaged neuronal filopodia dynamics in the absence of vessels and, endothelial filopodia in the absence of neurons. In *clo* mutant embryos, the number of neuronal filopodia was drastically reduced (Fig. 3d,d'). In contrast, in *neurog1* mutant embryos the number of EC filopodia did not change, though they were shorter (Fig. 3e-e''). These data indicate that neuronal filopodia require signals from ECs.

While sensory neurons in SAG do not appear to be required for vascular development, our data indicate that vasculature is required for SAG neurons to proliferate during a temporal window that coincides with the period of filopodial contacts. Moreover, neuroblasts only extend filopodia when ECs are present. Altogether, the results support the hypothesis that endothelial-neuronal filopodia contacts are required for vessels to signal to neuroblasts in the SAG to restrict growth.

bioRxiv preprint doi: https://doi.org/10.1101/667519; this version posted June 11, 2019. The copyright holder for this preprint (which was not certified by peer review) is the author/funder. All rights reserved. No reuse allowed without permission.

Cell signaling mediated by filopodia regulates the number of SAG neuroblasts

Cell signaling through filopodia has emerged as a novel mechanism of signaling between adjacent cells in different embryonic tissues[36–38]. In order to assess the possible role of filopodial signaling in SAG growth, filopodia formation was inhibited with LatrunculinB (LatB), a toxin that binds to actin and has been used to impair filopodia function *in vivo*[39,40]. Imaging and quantification of filopodia in embryos treated with LatB for 6 hours indicated that the treatment was effective, the number of filopodia in ECs and in neuroblasts was reduced (Fig. 4a,b). Interestingly, inhibition of filopodia caused an increased number of Neurod$^+$ cells in LatB-treated embryos and this phenotype was also due to a higher number of Neurod$^+$ cells incorporating BrdU (Fig. 4c-e). No additional effects were found in treated *clo* mutant embryos (Fig. 4c-e). Hence, filopodia formation inhibition at early stages recapitulated the SAG growth phenotype found previously in the avascular mutant. These data support the hypothesis that the endothelial-neuronal filopodial contacts exert a signaling role onto SAG neuroblast proliferation.

Dll4 inhibition increases the Neurod$^+$ population

To identify signals that could mediate the neurovascular crosstalk we revisited the published vascular signals regulating CNS neurogenesis for evidence of ligand expression in cranial vasculature or receptors in cranial sensory neurons[41]. In the Ventricular-Subventricular Zone (V-SVZ) of the adult brain, endothelial Jagged1 ligand restrains NSC proliferation[8]. Cranial vessels do not express Jagged1 but do express Delta-like 4 (Dll4), another Notch ligand, which is essential for proper vascular remodeling and sprouting[42–44]. We therefore hypothesized that Dll4 could be signaling to SAG neurons, which express Notch1 at the same early timepoints [45,46]. Moreover, it has been postulated that pigmentation patterning in zebrafish is regulated by DeltaC-Notch signaling through filopodia[47].

To test this hypothesis, we inhibited *dll4* through the well-studied *dll4* morpholino (MO)[43,44] and assessed its effects on SAG growth. Remarkably, *dll4* morphant embryos presented an expansion of the Neurod$^+$ population similar to the one observed previously in *clo* mutant embryos (Fig. 5a). This expansion was reflected both in SAG volume (Fig. 5b) as well as in Neurod$^+$ cell number (Fig. 5c). As a further control, *dll4* morpholino was also injected in *clo* mutant embryos and the number of Neurod$^+$ cells did not change, suggesting that the results are due to loss of *dll4* expressed by the vasculature (Fig. 5a-c). These findings reveal that Dll4 is required to regulate Neurod$^+$ cell number.

bioRxiv preprint doi: https://doi.org/10.1101/667519; this version posted June 11, 2019. The copyright holder for this preprint (which was not certified by peer review) is the author/funder. All rights reserved. No reuse allowed without permission.

In angiogenic sprouts, the number of filopodia increases after *dll4* downregulation[48]. When we assessed the number of filopodia in the developed PHBC, we detected a small increase in filopodial number and no differences in their length (Fig. 5d-f). Thus, the increase of Neurod$^+$ cells in *dll4* morphants cannot be attributed to a lack of filopodial processes but to a specific lack of signal. Finally, the number of ECs did not change in *dll4* morphant embryos compared to embryos injected with a random morpholino (Fig. 5g,h). Therefore, the increase in Neurod$^+$ cell number after *dll4* down-regulation is not due to vascular developmental changes but to Dll4-Notch1 signaling.

Together, these results suggest that Dll4 signaling constitutes one of the key molecular mechanisms by which the vasculature regulates cranial sensory neurogenesis.

Absence of vasculature impairs sensory neuronal differentiation

Since more neuroblasts form in the SAG in the absence of vasculature, we next assessed if these neuroblasts differentiate, resulting in a higher number of Islet2$^+$ post-mitotic cells at later stages. Unexpectedly we found, after plotting the number of immunostained Islet2$^+$ nuclei at different timepoints, that there was a significantly lower number of Islet2$^+$ cells in *clo* mutants from 54 hpf onwards (Fig. 6a,b). The differentiation curves indicate that, while at early timepoints sensory differentiation occurs partially independently of vasculature, from 54 hpf onwards, cranial vasculature is required to promote differentiation of Neurod$^+$ cells to Islet2$^+$ cells. As expected from the immunostaining data, the fluorescence from sensory axons was also reduced in *clo* mutant embryos, labelled by the *Tg(isl2:GFP)* ^{zc7} reporter line which marks *in vivo* the cytoplasm of differentiated sensory neurons[49] (Fig. 6c).

To determine if cranial vasculature regulates neurogenesis in other sensory ganglia besides the SAG, we assessed for filopodia contacts and quantified the number of Neurod$^+$ and Islet2$^+$ cells in different ganglia. Here, we did not perform a temporal analysis, but we chose discrete timepoints. At 30 hpf, we could also detect filopodia from the PHBC to the trigeminal and anterior lateral line ganglia (Supplementary Fig. 4c). At 36 hpf, we found a significantly increased number of Neurod$^+$ cells in the trigeminal ganglion of *clo* mutants (Supplementary Fig. 4a,b), whereas at 72 hpf there was a reduced number of Islet2$^+$ cells in the trigeminal and vagal ganglia (Supplementary Fig. 3d-g). Therefore, the neurovascular interaction appears to extend to other sensory ganglia.

To complete the analysis, we assessed if vasculature could regulate the development of other cell types such as the hair cells of the inner ear. For this aim, we generated *clo* homozygous mutants in the *Tg(brn3c:mGFP)* ^{s356t} background that labels the membranes of hair cells and

bioRxiv preprint doi: https://doi.org/10.1101/667519; this version posted June 11, 2019. The copyright holder for this preprint (which was not certified by peer review) is the author/funder. All rights reserved. No reuse allowed without permission.

their kinocilia[50]. Serial confocal stacks taken at 72 hpf and quantification of hair cells did not reveal significant differences in hair cell number in cristae nor maculae of *clo* mutants compared to siblings (Fig. 6d-f). Therefore, vasculature is specifically affecting neuronal differentiation of the inner ear but not hair cell number.

Initiation of blood flow triggers sensory differentiation

It has been reported that in zebrafish blood flow begins due to the completion of anastomosis of cranial blood vessels around 48 to 60 hpf[51]. The coincidence of this timing with the one of sensory differentiation defects in *clo* mutant embryos prompted us to explore whether the inducing signal of sensory differentiation was linked to blood flow. To this aim, we incubated embryos with Nifedipine, a drug that inhibits heartbeat and blood flow[52]. As expected from blood flow inhibition, we observed a drastic vessel diameter reduction in Nifedipine-treated embryos (Fig. 7a,b). In embryos treated with Nifedipine from 54 to 72 hpf, the number of Islet2^{+} cells decreased, recapitulating the defects found in *clo* mutant embryos (Fig. 7c-e). Treatment in the avascular model did not further enhance the phenotype, suggesting that the differentiation arrest is mostly attributed to the absence of blood flow in *clo* mutant embryos and not associated to side effects of Nifepidine (Fig. 7e). The same results were obtained when treatment was done with BDM, another drug used to inhibit blood flow[53] (Supplementary Fig. 5). To narrow down the time window of blood flow requirement, we incubated embryos with Nifedipine from 60 to 72 hpf and from 48 to 60 hpf. Incubation from 60 to 72 hpf did not inhibit differentiation (Fig. 7f,g), whereas incubation from 48 to 60 hpf did (Fig. 7h,i). These results indicate that blood flow disruption of sensory differentiation takes place in a narrow time window and once signaling is initiated, blood flow is no longer required.

Altogether, the results define for the first time a prominent role of cranial vasculature in sensory neurogenesis that can be segregated into two sequential and independent mechanisms. A first one, in which Dll4-Notch1 filopodia signaling from ECs to neurons regulates neuroblast transit-amplification, and a second one in which initiation of blood flow in vessels induces sensory neuron differentiation (Fig. 8).

Discussion

The SAG and other cranial sensory ganglia reside in a vascularized milieu in adults and during embryogenesis. A fundamental question in developmental neurobiology is whether or not vasculature, in addition to transport of nutrients and oxygen, provides instructive cues for

bioRxiv preprint doi: https://doi.org/10.1101/667519; this version posted June 11, 2019. The copyright holder for this preprint (which was not certified by peer review) is the author/funder. All rights reserved. No reuse allowed without permission.

sensory neurogenesis. This is relevant to understand hearing loss and other sensory neuropathies linked to vascular defects[54–56]. Our detailed temporal analysis reveals that cranial ganglia indeed require vascular signals for proper growth and differentiation. We identified two segregated mechanisms: an early filopodial-based, cell-cell contact dependent mechanism regulating neuroblast proliferation and a later blood flow-dependent mechanism controlling neuronal differentiation.

In the V-SVZ, quiescent NSCs physically contact blood vessels with specialized endfeet[7]. By taking advantage of the imaging and cell reporter tools available in the zebrafish model we resolve, for the first time, that cell-cell communication takes place through dynamic filopodial extensions that project from ECs to neuroblasts. It is still possible that in other contexts, dynamic contacts also exist, but imaging in fixed tissue might have hampered their identification, as suggested by Obernier and colleagues[57]. Filopodia in angiogenic tip cells and migrating ECs have been described[40,58–60]. To our knowledge, filopodia from endothelial stalk cells contacting neuronal cells have not been reported before. One could envision cell-cell contact with only ECs extending filopodia to neuronal somas. Interestingly, neuroblasts also emit filopodia, probably to increase the chances of cell-cell communication. Moreover, the study highlights the requirement of EC signals for neuronal filopodia growth.

Signaling roles for filopodia in *Drosophila* and vertebrates have been demonstrated, extending the cell-cell signaling distance of influence[36–38]. This is relevant in the facial mesenchyme where vasculature does not grow inside the sensory ganglia but adjacent. By blocking filopodia projections, we demonstrate that they have a signaling function in the negative control of neuroblast cell proliferation. Most likely only a subset of neuroblasts are contacted by endothelial filopodia, allowing a scattered pattern of cell cycle-arrested neuroblasts between others with proliferative capacities. In contrast to other contexts in which neurons control vascular patterning[61], our results suggest that in the context of sensory ganglia and surrounding vessels, an absence of cranial ganglia does not have a major effect on early vasculogenesis.

During adult neurogenesis, cell contact-dependent neurovascular signaling is mediated by ephrinB2 and Jagged1 present in ECs that suppress cell-cycle entry in NSCs[8]. We propose that in the PNS Dll4, but not Jagged1, plays a similar role. Maintenance of a quiescent and undifferentiated population of neural progenitors is key for life-long regeneration. Thus, the role we have uncovered for cranial vasculature and Dll4 in the cranial sensory niche might be relevant in regenerative studies upon neuronal damage.

bioRxiv preprint doi: https://doi.org/10.1101/667519; this version posted June 11, 2019. The copyright holder for this preprint (which was not certified by peer review) is the author/funder. All rights reserved. No reuse allowed without permission.

Several studies have highlighted the role of blood flow initiation in remodeling the vasculature, VEGF expression, angiogenesis and stimulation of hematopoietic stem cell formation[44,62,63]. It has been suggested that blood flow can exert tangential and perpendicular forces on ECs leading to actomyosin rearrangements, YAP-TAZ nuclear translocation and the induction of the mechano-sensitive transcription factor Klf2a[63–65]. Ultimately, blood flow triggers gene transcriptional changes in ECs and vessel maturation[66]. It is tempting to speculate that in our system, blood flow also triggers mechanical changes in ECs leading to the release of neuronal differentiation signals. Although we believe less plausible, expansion of the vasculature could also directly induce sensory differentiation by compression of the neuronal environment. Further studies should explore more precisely the changes taking place in cranial vessels upon blood flow initiation.

Our current work identifies novel roles for head vasculature and shall contribute to our basic understanding of the signalling mechanisms regulating sensory neurogenesis in which head vasculature enters in scene.

Acknowledgments

We thank D Stainer for the *Tg(cloche)*^{m378} and *Tg(kdrl:ras-mCherry)*^{s896} lines, the PRBB Imaging Facility for technical support, T Schilling, A Bigas and I Fariñas for comments on the manuscript and lab members for discussions. The work was supported by BFU2014-53203 and BFU2017-82723P from MCINN to BA and the Unidad de Excelencia Maria de Maeztu (MDM-2014-0370).

Methods

Zebrafish Strains and Genotyping

Zebrafish (*Danio rerio*) were maintained as previously described[67] at the aquatic facility of the Parc de Recerca Biomèdica de Barcelona (PRBB). The following transgenic lines in different combinations were used: *Tg(neurog1)*^{hi1059} [68] mutant to inhibit neurogenesis and *Tg(cloche)*^{m378} [69] as an avascular model. Five different reporter lines were used: *Tg(Kdrl:ras-mCherry)*^{s896} [70] and *Tg(flk1:EGFP)*^{s843} [71] for vessels , *TgBAC(neurod:EGFP)*^{nl1} [72] for neuroblasts, *Tg(isl2:gfp)*^{zc7} (also called Isl3)[49] for sensory differentiated neurons and *Tg(brn3c:mGFP)*^{s356t} [50] for hair cells .

Embryos were staged as previously described [73]. Adult heterozygous for *neurog1*^{hi1059} allele were identified by PCR genotyping by fin-clip genomic DNA[68]. Homozygous *neurog1* mutant embryos were recognized by the significant reduction of GFP signal in *Tg(neurog1)*^{hi1059}*, BAC(neurod:EGFP)*^{nl1}*, (Kdrl:ras-mCherry)*^{s896} background. Avascular mutants were identified

bioRxiv preprint doi: https://doi.org/10.1101/667519; this version posted June 11, 2019. The copyright holder for this preprint (which was not certified by peer review) is the author/funder. All rights reserved. No reuse allowed without permission.

by the lack of vasculature in the reporter line for endothelial cells *Tg(Kdrl:ras-mCherry)* ^{s896} or *Tg(flk-1:EGFP)* ^{s843}, lack of blood cells and circulation (visible under scope from 30-36hpf) and atrium enlargement, as described by Stainer et al. [29].

In both cases, wild-type and heterozygous-deficient siblings were undistinguishable and both have been used and referred as siblings (sib). Finally, since *clo* mutant embryos die around 7dpf [69], we studied embryos until 4dpf to exclude vessel directed effects from embryonic morbidity.

Live imaging, confocal microscopy and quantifications

Images of cryosections were acquired with a Leica DFC 7000 T microscope, and 40x oil immersion (0.75 NA).

Whole-mount embryos imaging was performed on a Leica SP8 confocal microscope, with 20x glycerol immersion lens (0.7 NA). Embryos were mounted in 1% low-melting agarose (Ecogene) in PBS or Danieau's solution, for fixed and life embryos respectively, and placed onto a glass-bottom dish. For life embryos, 0.1% Tricaine (Sigma) was also added. The 488- and 561-nm laser lines were employed at a scan speed of 600 Hz.

For time-lapse imaging of filopodial, the resonant mode (8000 Hz) was used to achieve a high spatiotemporal resolution. Frames were captured simultaneously with 488 nm and 561 nm lasers at a time interval of 15 seconds. Z-size of 2 µm was used for videos and 0.5 µm for static stacks and transverse optical reconstructions. Confocal stacks and movies were flattened by maximum projections using FIJI (Image J).

Measurements were done manually with FIJI (Image J) for SAG and PHBC filopodia number, length and orientation using one single static image, from a defined region of interest (ROI). PHBC width was measured from maximum projection confocal images always at the same point, between CtA 2 and 3. PHBC EC number was calculated by perinuclear green cytosolic signalling from *Tg(flk-1:EGFP)* ^{s843} and EC contours from *Tg(Kdrl:ras-mCherry)* ^{s896} in a defined ROI. When ROIs were used, the same area was used to compare samples. SAG anteroposterior (AP) and dorsoventral (DV) axes length were measured from maximum projection confocal lateral images. The mediolateral (ML) SAG axis was calculated from 5 serial cryosections, in which the biggest measurement was used.

The number of Neurod^{+} nuclei was counted manually using DAPI staining in the *TgBAC(neurod:egfp)* ^{nl1} labelled cells. *neurog1*$^{+}$ cells were also counted manually after an ISH and DAPI staining. The number of HC was calculated using the *Tg(brn3c:mGFP)* ^{s356t} and counting kinocilia number.

bioRxiv preprint doi: https://doi.org/10.1101/667519; this version posted June 11, 2019. The copyright holder for this preprint (which was not certified by peer review) is the author/funder. All rights reserved. No reuse allowed without permission.

The volume of the SAG was measured by calculating the area the 5 serial cryosections that include all SAG and multiplying them with each section thickness (20µm).

Statistical Analysis

All the data in the work were first tested for normal distribution using the Kolmogorov-Smirnov test and the Levene's test for homogeneity of variances. For two-group comparison two-tailed Student's *t*-test was used or Mann-Whitney *U* test for non-parametric tests. When more than two samples were being compared, one-way ANOVA followed by post-hoc test was performed. Values are expressed as median ± SEM. Graphs were performed with PRISM 7 (Graph-Pad) software. Error bars represent SEM, but for Fig. 2d and Fig. 5a, were shaded error bars represent SD. ns= non-significant, *p≤0.05, **p≤0.01, ***p≤0.001.

Immunostaining and *in situ* Hybridization

Embryos at the desired stage were fixed with 4% paraformaldehyde (PFA) in PBS 0,1% Tween-20 (PBT) for 3 hours at RT or overnight at 4ºC. Fixed embryos were dehydrated, kept in 100% MeOH -20ºC 1h or overnight (O/N), and rehydrated. Embryos were permeabilized with Proteinase K 1:1000 in PBT, or cold Acetone for mouse anti-Islet1/2, and incubated with blocking solution (BS) for 2h at room temperature (RT) and with primary antibody O/N at 4ºC. Primary antibody was washed 5 times 10min, and secondary antibody was applied for 2h RT or O/N 4ºC.

Embryos were cryoprotected in 15% sucrose and embedded in 7.5% gelatine/15% sucrose. Blocks were frozen in 2-methylbutane (Sigma) to improve tissue preservation. Sagittal and transversal sections were cut at 20µm thickness in a Leica CM 1950 cryostat.

For BrdU incorporation experiments, dechorionated live embryos were incubated with 10mM BrdU, 10% DMSO in Danieau's solution for 6 hours. After this they were washed twice in clean Danieau's solution for 5 min prior 4% PFA fixation for 3 hours at RT. BrdU staining was performed in cryosections after 2N HCl DNA denaturation 1h RT. Anti-BrdU (bdbiosciences; mouse Cat: 555627, 1:100). Anti-GFP was used to enhance GFP signal from transgenic lines (Torrey Pines BioLabs Inc; rabbit Cat: TP401, 1:400). Anti-Islet1/2 was used to detect differentiated neurons (Cat: TP401; mouse Cat: 39.4D5, 1:200). Alexa-fluor 488 and 594 anti-rabbit and anti-mouse (Invitrogen, 1:400) were used as secondary antibodies. DAPI staining for cryosections was done at 1:10000 PBS for 5min, and 2x5min wash in PBS followed by mowiol mounting.

bioRxiv preprint doi: https://doi.org/10.1101/667519; this version posted June 11, 2019. The copyright holder for this preprint (which was not certified by peer review) is the author/funder. All rights reserved. No reuse allowed without permission.

Whole-mount *in situ* hybridization was performed as previously described[74] using *neurog1* digoxigenin-labelled probe.

Inhibitor treatments

To block actin polymerization in filopodia, dechorionated live embryos were incubated in 0,1µg/mL Latrunculin B (LatB) (Merk, Millipore), 0,4% DMSO in Danieau's solution for 6 hours[40]; while control embryos were raised at 0,4% DMSO only. After treatment, embryos were washed twice in clean Danieau's solution for 5min followed by immediate confocal imaging for filopodia visualization or 4% PFA fixation. In other cases, embryos were washed in Danieau's solution until 36 hpf. It has been previously demonstrated that the concentration used of LatB specifically inhibits filopodial formation while it does not affect other cellular behaviours for up to 17 hours of treatment[40].

Blood flow was blocked through the use of two different drugs. Dechorionated live embryos were incubated for 6, 12 and 24 hours in 40µM Nifedipine or 20mM BDM (2, 3-butanedione-2-monoxime) (Sigma-Aldrich) in Danieau's solution, washed twice 5min and fixed in 4% PFA at the desired stage[52,53].

Morpholino knockdown experiments

To inhibit protein translation of Dll4, 10ng of random and *dll4* splicing morpholino antisense oligonucleotides (Gene Tools, Philomath, OR) were injected in the yolk of 1-2 cell stage embryos as previously described[43]. Efficiency of the knockdown was assessed by RT-PCR (data not shown).

References

1. Fuentealba, L. C., Obernier, K. & Alvarez-Buylla, A. Adult neural stem cells bridge their niche. *Cell Stem Cell* **10**, 698–708 (2012).

2. Silva-Vargas, V., Crouch, E. E. & Doetsch, F. Adult neural stem cells and their niche: a dynamic duo during homeostasis, regeneration, and aging. *Curr. Opin. Neurobiol.* **23**, 935–942 (2013).

3. Otsuki, L. & Brand, A. H. The vasculature as a neural stem cell niche. *Neurobiol. Dis.* **107**, 4–14 (2017).

4. Shen, Q. *et al.* Adult SVZ Stem Cells Lie in a Vascular Niche: A Quantitative Analysis of Niche Cell-Cell Interactions. *Cell Stem Cell* **3**, 289–300 (2008).

5. Mirzadeh, Z., Merkle, F. T., Soriano-Navarro, M., Garcia-Verdugo, J. M. & Alvarez-Buylla, A. Neural Stem Cells Confer Unique Pinwheel Architecture to the Ventricular Surface in Neurogenic Regions of the Adult Brain. *Cell Stem Cell* **3**, 265–278 (2008).

bioRxiv preprint doi: https://doi.org/10.1101/667519; this version posted June 11, 2019. The copyright holder for this preprint (which was not certified by peer review) is the author/funder. All rights reserved. No reuse allowed without permission.

6. Palmer, T. D., Willhoite, A. R. & Gage, F. H. Vascular Niche for Adult Hippocampal Neurogenesis. *J. Comp. Neurolgy* **494**, 479–494 (2000).

7. Tavazoie, M. *et al.* A Specialized Vascular Niche for Adult Neural Stem Cells. *Cell Stem Cell* **3**, 279–288 (2008).

8. Ottone, C. *et al.* Direct cell-cell contact with the vascular niche maintains quiescent neural stem cells. *Nat. Cell Biol.* **16**, 1045–1056 (2014).

9. Louissaint, A., Rao, S., Leventhal, C. & Goldman, S. Coordinated interaction of neurogenesis and angiogenesis in the adult songbird brain. *Neuron* **34**, 945–960 (2002).

10. Androutsellis-Theotokis, A. *et al.* Targeting neural precursors in the adult brain rescues injured dopamine neurons. *Proc. Natl. Acad. Sci.* **106**, 13570–13575 (2009).

11. Jin, K., Mao, X. O., Sun, Y., Xie, L. & Greenberg, D. A. Stem cell factor stimulates neurogenesis in vitro and in vivo. *J. Clin. Invest.* **110**, 311–319 (2002).

12. Ramírez-Castillejo, C. *et al.* Pigment epithelium-derived factor is a niche signal for neural stem cell renewal. *Nat. Neurosci.* **9**, 331–339 (2006).

13. Calvo, C. F. *et al.* Vascular endothelial growth factor receptor 3 directly regulates murine neurogenesis. *Genes Dev.* **25**, 831–844 (2011).

14. Delgado, A. C. *et al.* Endothelial NT-3 Delivered by Vasculature and CSF Promotes Quiescence of Subependymal Neural Stem Cells through Nitric Oxide Induction. *Neuron* **83**, 572–585 (2014).

15. Tan, X. *et al.* Vascular Influence on Ventral Telencephalic Progenitors and Neocortical Interneuron Production. *Dev. Cell* **36**, 624–638 (2016).

16. Tata, M. *et al.* Regulation of embryonic neurogenesis by germinal zone vasculature. *Proc. Natl. Acad. Sci.* **113**, 13414–13419 (2016).

17. Lange, C. *et al.* Relief of hypoxia by angiogenesis promotes neural stem cell differentiation by targeting glycolysis. *EMBO J.* **35**, 924–941 (2016).

18. Ma, Q., Chen, Z., Barrantes, I. del B., Luis de la Pompa, J. & Anderson, D. J. Neurogenin1 Is Essential for the Determination of Neuronal Precursors for Proximal Cranial Sensory Ganglia. *Neuron* **20**, 469–482 (1998).

19. Liu, M. *et al.* Loss of BETA2/NeuroD leads to malformation of the dentate gyrus and epilepsy. *Proc. Natl. Acad. Sci.* **97**, 865–870 (2000).

20. Maier, E. C., Saxena, A., Alsina, B., Bronner, M. E. & Whitfield, T. T. Sensational placodes: Neurogenesis in the otic and olfactory systems. *Dev. Biol.* **389**, 50–67 (2014).

21. Begbie, J., Ballivet, M. & Graham, A. Early Steps in the Production of Sensory Neurons by the Neurogenic Placodes. *Mol. Cell. Neurosci.* **21**, 502–511 (2002).

22. Bilak, M. M., Hossain, W. A. & Morest, D. K. Intracellular fibroblast growth factor produces effects different from those of extracellular application on development of avian cochleovestibular ganglion cells in vitro. *J. Neurosci. Res.* **71**, 629–647 (2003).

23. Camarero, G. *et al.* Insulin-like growth factor 1 is required for survival of transit-amplifying neuroblasts and differentiation of otic neurons. *Dev. Biol.* **262**, 242–253 (2003).

bioRxiv preprint doi: https://doi.org/10.1101/667519; this version posted June 11, 2019. The copyright holder for this preprint (which was not certified by peer review) is the author/funder. All rights reserved. No reuse allowed without permission.

24. Vemaraju, S., Kantarci, H., Padanad, M. S. & Riley, B. B. A Spatial and Temporal Gradient of Fgf Differentially Regulates Distinct Stages of Neural Development in the Zebrafish Inner Ear. *PLoS Genet.* **8**, e1003068 (2012).

25. Fantetti, K. N. & Fekete, D. M. Members of the BMP, Shh, and FGF morphogen families promote chicken statoacoustic ganglion neurite outgrowth and neuron survival in vitro. *Dev. Neurobiol.* **72**, 1213–1228 (2012).

26. Murdoch, B. & Roskams, A. J. Fibroblast Growth Factor Signaling Regulates Neurogenesis at Multiple Stages in the Embryonic Olfactory Epithelium. *Stem Cells Dev.* **22**, 525–537 (2012).

27. Alsina, B., Giraldez, F. & Varela-Nieto, I. Growth Factors and Early Development of Otic Neurons: Interactions between Intrinsic and Extrinsic Signals. *Curr. Top. Dev. Biol.* **57**, 177–206 (2003).

28. Taberner, L., Bañón, A. & Alsina, B. Anatomical map of the cranial vasculature and sensory ganglia. *J. Anat.* **232**, 431–439 (2018).

29. Stainier, D. Y., Weinstein, B. M., Detrich, H. W., Zon, L. I. & Fishman, M. C. Cloche, an early acting zebrafish gene, is required by both the endothelial and hematopoietic lineages. *Development* **121**, 3141–50 (1995).

30. Reischauer, S. *et al.* Cloche is a bHLH-PAS transcription factor that drives haemato-vascular specification. *Nature* **535**, 294–298 (2016).

31. Liao, W., Bisgrove, B., Sawyer, H. & Hug, B. The zebrafish gene cloche acts upstream of a flk-1 homologue to regulate endothelial cell differentiation. *Development* **124**, 381–389 (1997).

32. Sumanas, S., Jorniak, T. & Lin, S. Identification of novel vascular endothelial-specific genes by the microarray analysis of the zebrafish cloche mutants. *Blood* **106**, 534–541 (2005).

33. Mukouyama, Y., Shin, D., Britsch, S., Taniguchi, M. & Anderson, D. J. Sensory Nerves Determine the Pattern of Arterial Differentiation and Blood Vessel Branching in the Skin. *Cell* **109**, 693–705 (2002).

34. Makita, T., Sucov, H. M., Gariepy, C. E., Yanagisawa, M. & Ginty, D. D. Endothelins are vascular-derived axonal guidance cues for developing sympathetic neurons. *Nature* **452**, 759–763 (2008).

35. Barber, M. *et al.* Vascular-derived VEGFA promotes cortical interneuron migration and proximity to the vasculature in the developing forebrain. *Cereb. Cortex* **28**, 2577–2593 (2018).

36. Kornberg, T. B. Distributing signaling proteins in space and time: the province of cytonemes. *Curr. Opin. Genet. Dev.* **45**, 22–27 (2017).

37. Stanganello, E. *et al.* Filopodia-based Wnt transport during vertebrate tissue patterning. *Nat. Commun.* **6**, 1–14 (2015).

38. Stanganello, E. & Scholpp, S. Role of cytonemes in Wnt transport. *J. Cell Sci.* **129**, 665–672 (2016).

39. Morton, W. M., Ayscough, K. R. & McLaughlin, P. J. Latrunculin alters the actin-monomer subunit interface to prevent polymerization. *Nat. Cell Biol.* **2**, 376–378 (2000).

40. Phng, L.-K., Stanchi, F. & Gerhardt, H. Filopodia are dispensable for endothelial tip cell

bioRxiv preprint doi: https://doi.org/10.1101/667519; this version posted June 11, 2019. The copyright holder for this preprint (which was not certified by peer review) is the author/funder. All rights reserved. No reuse allowed without permission.

guidance. *Development* **140**, 4031–4040 (2013).

41. Howe DG, Bradford YM, Conlin T, Eagle AE, Fashena D, Frazer K, Knight J, Mani P, Martin R, Moxon SA, Paddock H, Pich C, Ramachandran S, Ruef BJ, Ruzicka L, Schaper K, Shao X, Singer A, Sprunger B, Van Slyke CE, W. M. ZFIN, the Zebrafish Model Organism Database: increased support for mutants and transgenics. *Nucleic Acids Res.* Jan;41(Database issue):D854-60. (2013).

42. Leslie, J. D. *et al.* Endothelial signalling by the Notch ligand Delta-like 4 restricts angiogenesis. *Development* **134**, 839–844 (2007).

43. Siekmann, A. F. & Lawson, N. D. Notch signalling limits angiogenic cell behaviour in developing zebrafish arteries. *Nature* **445**, 781–784 (2007).

44. Bussmann, J., Wolfe, S. A. & Siekmann, A. F. Arterial-venous network formation during brain vascularization involves hemodynamic regulation of chemokine signaling. *Development* **138**, 1717–1726 (2011).

45. Nikolaou, N. *et al.* Lunatic fringe promotes the lateral inhibition of neurogenesis. *Development* **136**, 2523–2533 (2009).

46. Fujita, M. *et al.* Assembly and patterning of the vascular network of the vertebrate hindbrain. *Development* **138**, 1705–1715 (2011).

47. Hamada, H. *et al.* Involvement of Delta/Notch signaling in zebrafish adult pigment stripe patterning. *Development* **141**, 318–324 (2014).

48. Suchting, S. *et al.* The Notch ligand Delta-like 4 negatively regulates endothelial tip cell formation and vessel branching. *Proc. Natl. Acad. Sci.* **104**, 3225–3230 (2007).

49. Pittman, A. J., Law, M.-Y. & Chien, C.-B. Pathfinding in a large vertebrate axon tract: isotypic interactions guide retinotectal axons at multiple choice points. *Development* **135**, 2865–2871 (2008).

50. Xiao, T., Roeser, T., Staub, W. & Baier, H. A GFP-based genetic screen reveals mutations that disrupt the architecture of the zebrafish retinotectal projection. *Development* **132**, 2955–2967 (2005).

51. Siekmann, A. F., Standley, C., Fogarty, K. E., Wolfe, S. A. & Lawson, N. D. Chemokine signaling guides regional patterning of the first embryonic artery. *Genes Dev.* **23**, 2272–2277 (2009).

52. Li, W. M., Webb, S. E., Chan, C. M. & Miller, A. L. Multiple roles of the furrow deepening Ca2+ transient during cytokinesis in zebrafish embryos. *Dev. Biol.* **316**, 228–248 (2008).

53. Anderson, M. J., Pham, V. N., Vogel, A. M., Weinstein, B. M. & Roman, B. L. Loss of unc45a precipitates arteriovenous shunting in the aortic arches. *Dev. Biol.* **318**, 258–267 (2008).

54. Lago, M. R. R. *et al.* Sensorineural hearing loss in children with sickle cell anemia and its association with endothelial dysfunction. *Hematology* **23**, 849–855 (2018).

55. Paul, A. *et al.* Isolated intermittent bilateral hearing loss revealing a brain hemorrhage. *J. Neurol. Sci.* **370**, 18–20 (2016).

56. Jensen, R. W., Chuman, H., Trobe, J. D. & Deveikis, J. P. Facial and Trigeminal Neuropathies in Cavernous Sinus Fistulas. *J. Neuro-Ophthalmology* **24**, 34–38 (2004).

57. Obernier, K. *et al.* Adult Neurogenesis Is Sustained by Symmetric Self-Renewal and Differentiation. *Cell Stem Cell* 221-234.e8 (2018). doi:10.1016/j.stem.2018.01.003

bioRxiv preprint doi: https://doi.org/10.1101/667519; this version posted June 11, 2019. The copyright holder for this preprint (which was not certified by peer review) is the author/funder. All rights reserved. No reuse allowed without permission.

58. Ochsenbein, A. M. *et al.* Endothelial cell-derived semaphorin 3A inhibits filopodia formation by blood vascular tip cells. *Development* **143**, 589–594 (2016).

59. Fantin, A. *et al.* NRP1 Regulates CDC42 Activation to Promote Filopodia Formation in Endothelial Tip Cells. *Cell Rep.* **11**, 1577–1590 (2015).

60. Gerhardt, H. *et al.* VEGF guides angiogenic sprouting utilizing endothelial tip cell filopodia. *J. Cell Biol.* **161**, 1163–1177 (2003).

61. Himmels, P. *et al.* Motor neurons control blood vessel patterning in the developing spinal cord. *Nat. Commun.* **8**, (2017).

62. Adamo, L. *et al.* Biomechanical forces promote embryonic haematopoiesis. *Nature* **459**, 1131–1135 (2009).

63. Nicoli, S. *et al.* MicroRNA-mediated integration of haemodynamics and Vegf signalling during angiogenesis. *Nature* **464**, 1196–1200 (2010).

64. Le Noble, F., Klein, C., Tintu, A., Pries, A. & Buschmann, I. Neural guidance molecules, tip cells, and mechanical factors in vascular development. *Cardiovasc. Res.* **78**, 232–241 (2008).

65. Nakajima, H. *et al.* Flow-Dependent Endothelial YAP Regulation Contributes to Vessel Maintenance. *Dev. Cell* **40**, 523-536.e6 (2017).

66. Chiu, J.-J. & Chien, S. Effects of Disturbed Flow on Vascular Endothelium: Pathophysiological Basis and Clinical Perspectives. *Physiol. Rev.* **91**, 327–387 (2011).

67. Westerfield, M. *The zebrafish book. A guide for the laboratory use of zebrafish (Danio rerio).* (Univ. of Oregon Press, Eugene., 2000).

68. Golling, G. *et al.* Insertional mutagenesis in zebrafish rapidly identifies genes essential for early vertebrate development. *Nat. Genet.* **31**, 135–140 (2002).

69. Stainier, D. Y. *et al.* Mutations affecting the formation and function of the cardiovascular system in the zebrafish embryo. *Development* **123**, 285–92 (1996).

70. Chi, N. C. *et al.* Foxn4 directly regulates tbx2b expression and atrioventricular canal formation. *Genes Dev.* 734–739 (2008). doi:10.1101/gad.1629408.734

71. Jin, S.-W., Beis, D., Mitchell, T., Chen, J.-N. & Stainier, D. Y. R. Cellular and molecular analyses of vascular tube and lumen formation in zebrafish. *Development* **132**, 5199–5209 (2005).

72. Obholzer, N. *et al.* Vesicular Glutamate Transporter 3 Is Required for Synaptic Transmission in Zebrafish Hair Cells. *J. Neurosci.* **28**, 2110–2118 (2008).

73. Kimmel, C. B., Ballard, W. W., Kimmel, S. R., Ullmann, B. & Schilling, T. F. CB_et_al-1995-Developmental_Dynamics. **10**, (1995).

74. Thisse, B. *et al.* Spatial and Temporal Expression of the Zebrafish Genome by Large-Scale In Situ Hybridization Screening. *Methods Cell Biol.* **77**, 505–519 (2004).

bioRxiv preprint doi: https://doi.org/10.1101/667519; this version posted June 11, 2019. The copyright holder for this preprint (which was not certified by peer review) is the author/funder. All rights reserved. No reuse allowed without permission.

Figures and Figure Legends

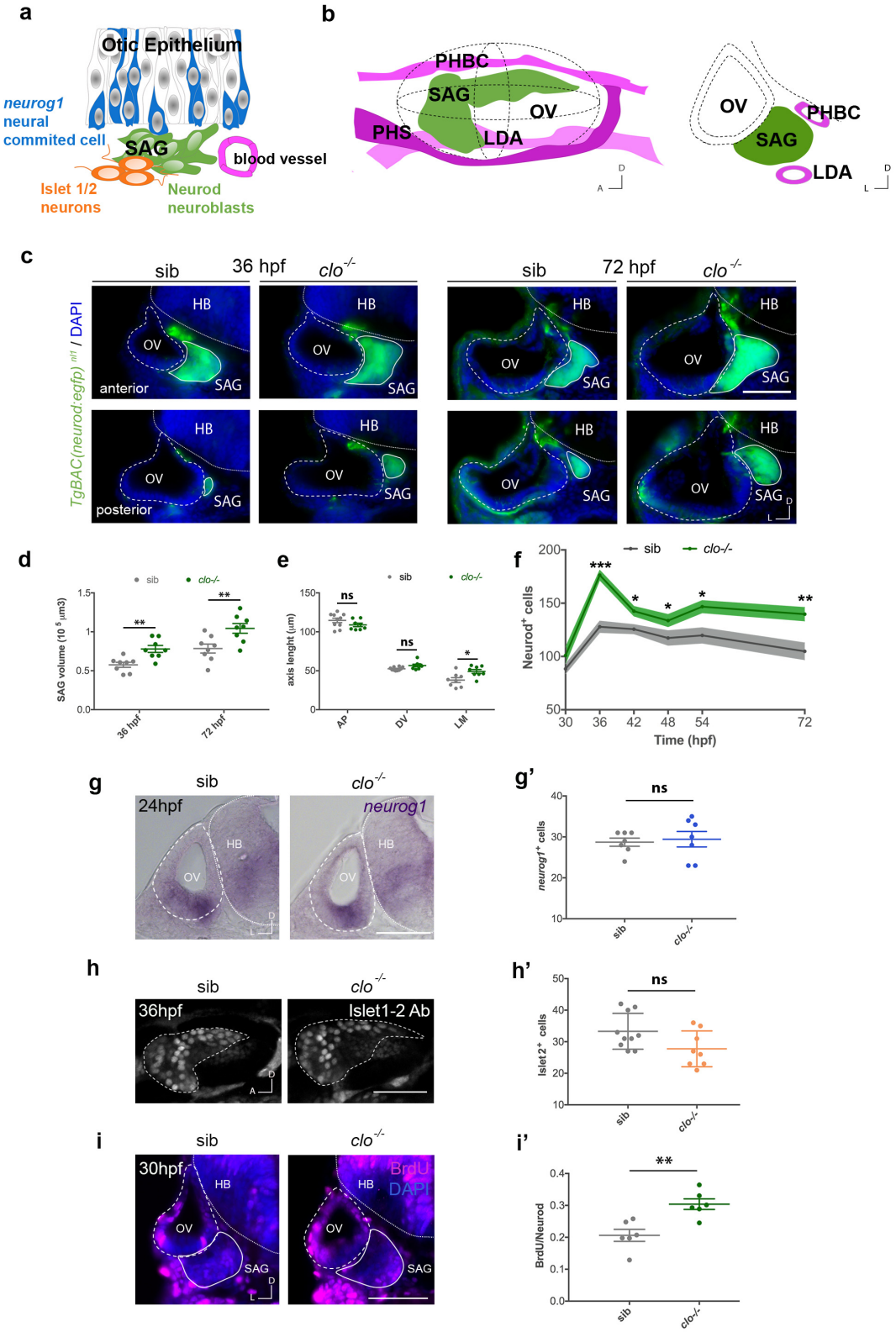

Figure 1. In the absence of vessels, the Neurod⁺ population in the SAG is expanded due to increased proliferation but not to effects on specification or differentiation.

a, Schematic drawing of the sequential steps of otic neurogenesis. Colored graphs representing effects in specific cell types will follow this scheme: neurog1⁺ neuronal

bioRxiv preprint doi: https://doi.org/10.1101/667519; this version posted June 11, 2019. The copyright holder for this preprint (which was not certified by peer review) is the author/funder. All rights reserved. No reuse allowed without permission.

committed progenitors in blue, Neurod^{+} neuroblasts in green, Islet1/2^{+} neurons in orange and blood vessels in magenta. **b**, Lateral (left) and transversal (right) 3D drawing of the OV (dotted line), the SAG and the adjacent vessels: PHBC, LDA and PHS. **c**, Representative anterior and posterior transverse images of the SAG in sib and clo$^{-/-}$ *TgBAC(neurod:egfp)* ^{nl1} embryos of cryostat sections, at 36 and 72 hpf. Neurod^{+} cells: green, neuroblasts; DAPI: blue, nuclei. **d**, Quantification of SAG volumes in sib and clo$^{-/-}$ embryos at 36 and 72 hpf (n=8). **e**, Graph showing measurements of the anteroposterior (AP), dorsoventral (DV) or mediolateral (ML) axis length of the SAG in sib and clo$^{-/-}$ embryos (n=8-10), at 72 hpf. **f**, Quantification of Neurod^{+} nuclei in the SAG visualized through the *TgBAC(neurod:egfp)* ^{nl1} of sib and clo$^{-/-}$ embryos at different timepoints from 30 to 72 hpf (n = 6-10). **g**, Transversal images of *neurog1 in situ* hybridization in the OV epithelium in sib and clo$^{-/-}$ embryos, at 24 hpf; and quantified in **g'** (n = 7). **h**, Confocal lateral images of immunostained Islet 1/2^{+} nuclei in the SAG (dotted line, visualized by *TgBAC(neurod:egfp)* ^{nl1}) in sib and clo$^{-/-}$ embryos, at 36 hpf; and quantified in **h'** (sib n = 10, clo$^{-/-}$ n = 8). **i**, Transversal images of BrdU incorporation (magenta) in the SAG (continuous line, visualized by *TgBAC(neurod:egfp)* ^{nl1}) in sib and clo$^{-/-}$ embryos, at 30 hpf; and quantified in **i'** (n = 6). DAPI: blue, nuclei. Scale bar, 50 µm. Error bars, mean ± SEM for **d**,**e**,**g'**,**h'**,**i'**; and mean ± SD for **f**. Unpaired two-tailed Student's *t*-test. * $p < 0.05$, ** $p < 0.01$, *** $p < 0.001$. ns, non-significant. OV, otic vesicle; SAG, statoacoustic ganglion; PHBC, primordial hindbrain channel; LDA, lateral dorsal aorta; PHS, primary head sinus; HB, hindbrain; sib, siblings.

bioRxiv preprint doi: https://doi.org/10.1101/667519; this version posted June 11, 2019. The copyright holder for this preprint (which was not certified by peer review) is the author/funder. All rights reserved. No reuse allowed without permission.

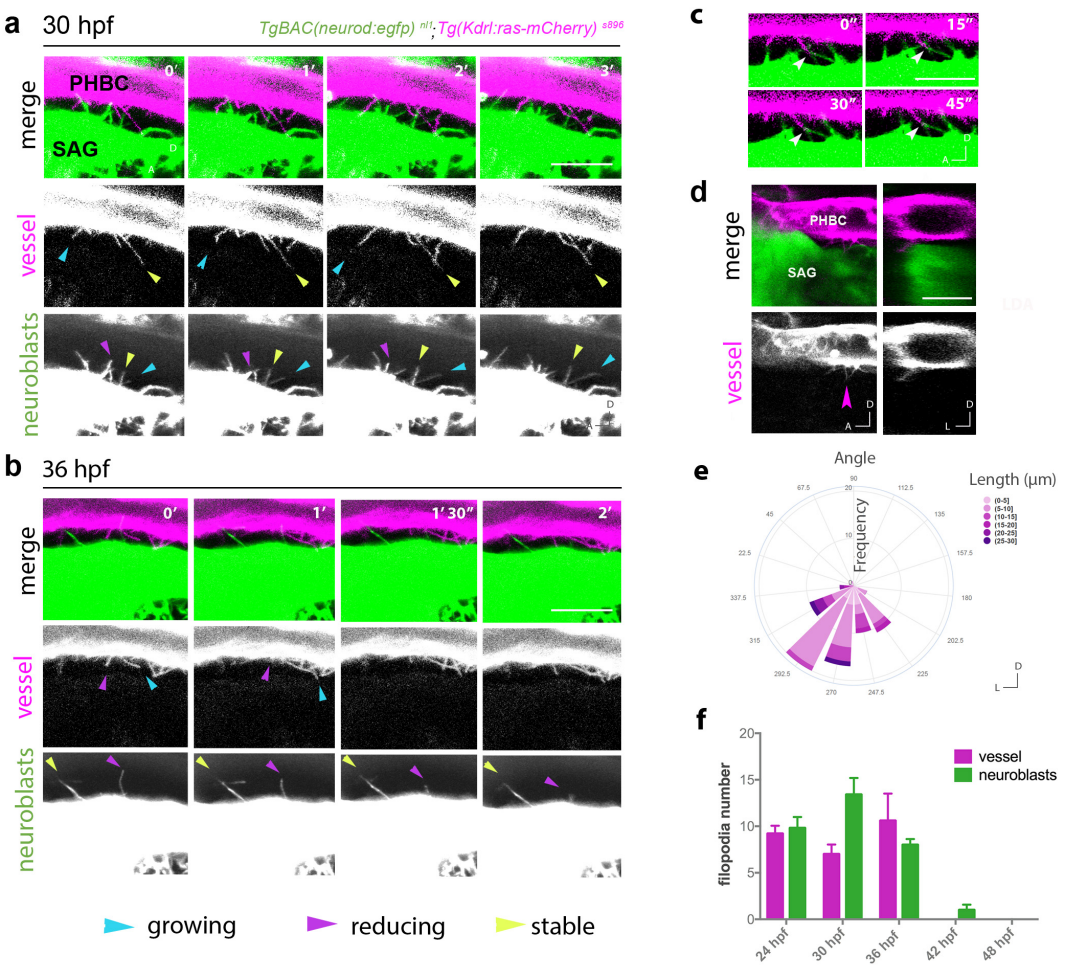

Figure 2. Endothelial cells and SAG neuroblasts contact through directional filopodia.
a,**b**, Timelapse of lateral images of *TgBAC(neurod:egfp)* ^{nl1}*; (Kdrl:ras-mCherry)* ^{s896} embryos showing filopodia extending from the PHBC to the SAG and from the SAG to the PHBC at 30 and 36 hpf (videos are representative of 5 experiments). Cyan, magenta and yellow arrowheads point to examples of growing, reducing and stable filopodia, respectively. **c**, 4 µm thick z-projection exemplifying a filopodia-filopodia contact remaining stable for more than 45 seconds, 30 hpf. **d**, Single plane images in lateral view and transversal optic reconstruction showing a filopodial process from the PHBC to the SAG, at 30 hpf. Arrowhead indicates point for transverse optical reconstruction. **e**, Rose plot of PHBC filopodia frequency of angle distribution and length (0º, lateral; 90º, dorsal; 180º, medial; 270º, ventral (n=76 filopodia, 15 embryos), at 30 hpf. **f**, Histogram showing the number of filopodia in the PHBC (magenta) and the SAG (green) at different timepoints from 24 to 48 hpf (n = 5). Scale bars, 20 µm in **a**,**b**,**d** and 10 µm in **c**. SAG, statoacoustic ganglion; PHBC, primordial hindbrain channel.

bioRxiv preprint doi: https://doi.org/10.1101/667519; this version posted June 11, 2019. The copyright holder for this preprint (which was not certified by peer review) is the author/funder. All rights reserved. No reuse allowed without permission.

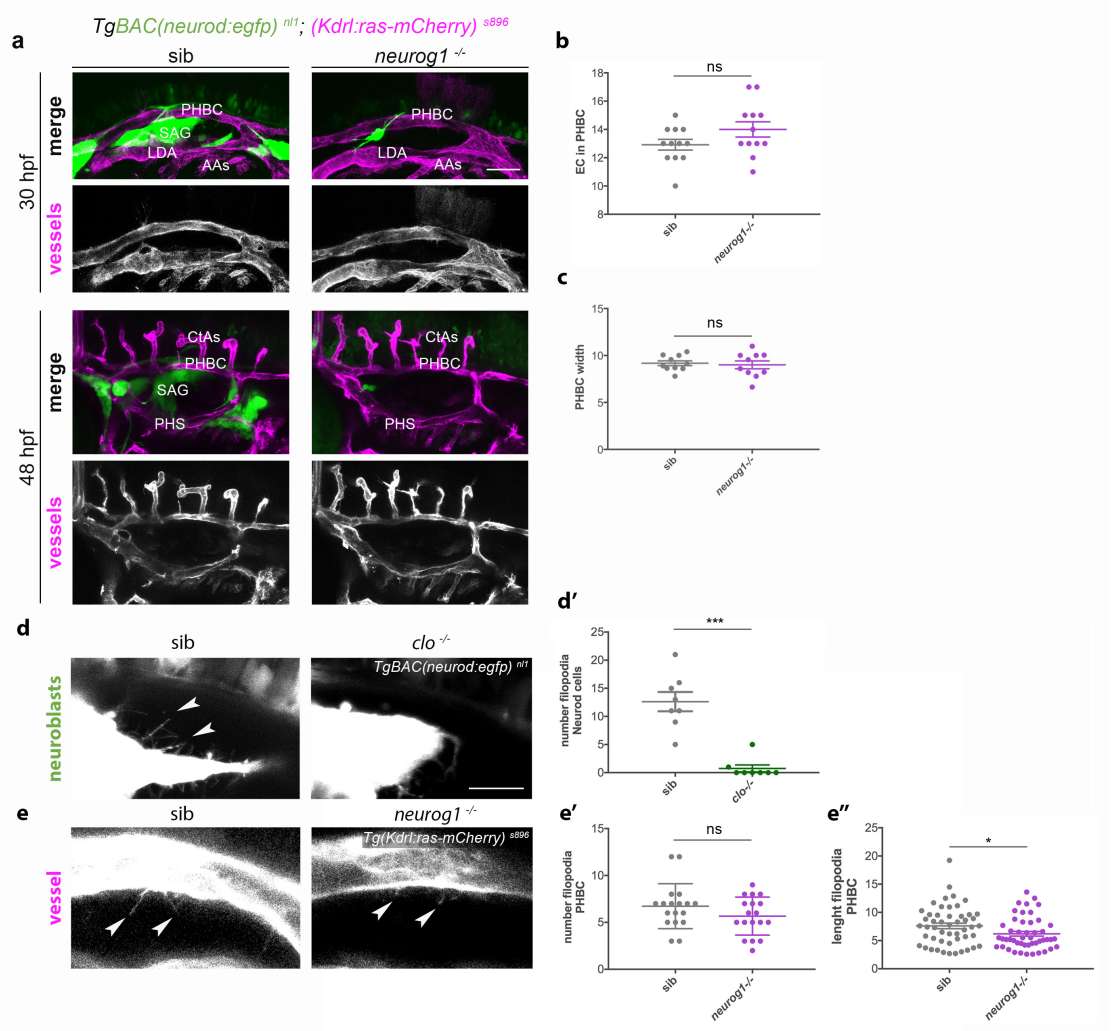

Figure 3. Lack of neurogenesis does not affect cranial vasculature patterning nor filopodia formation, while loss of vasculature prevents neuroblasts filopodia formation.

a, Representative lateral images of cranial vasculature in sib and *neurog1*$^{-/-}$ homozygous mutant embryos in *TgBAC(neurod:egfp)* ^{nls1}*, (Kdrl:ras-mCherry)* ^{s896} background, at 30 hpf and 48 hpf. **b**, Quantification of EC numbers in sib and *neurog1*$^{-/-}$ (n = 12), at 48 hpf. **c**, Quantification of PHBC width in sib and *neurog1*$^{-/-}$ (n = 10), at 48 hpf. **d**, Confocal lateral images showing neuroblasts filopodial processes visualized through the *TgBAC(neurod:egfp)* ^{nl1} in sib and clo $^{-/-}$, at 30 hpf. **d'**, Graph of SAG neuroblasts filopodia number in sib and clo $^{-/-}$ (n = 8), at 30 hpf. **e**, Confocal lateral images showing PHBC filopodial processes visualized through the *Tg(Kdrl:ras-mCherry)* ^{s896} in sib and *neurog1*$^{-/-}$ embryos, at 30 hpf. Arrowheads indicate filopodia in **d** and **e**. **e'**, Graph of PHBC filopodia number in sib and *neurog1*$^{-/-}$ (n = 18), at 30 hpf. **e''**, Graph of PHBC filopodia length in sib (n = 50) and *neurog1*$^{-/-}$ (n = 48), at 30 hpf.

Scale bars, 50 µm in **a** and 20 µm in **d,e**. Error bars, mean ± SEM. Unpaired two-tailed Student's *t*-test for **b, c, d', e'** and unpaired one-tailed Student's *t*-test for **e''**. * $p < 0.05$, ** $p < 0.01$, *** $p < 0.001$. ns, non-significant. PHBC, primordial hindbrain channel; LDA, lateral dorsal aorta; AAs, aortic arches; PHS, primary head sinus; CtAs, central arteries; SAG, statoacoustic ganglion; EC, endothelial cells; sib, siblings.

bioRxiv preprint doi: https://doi.org/10.1101/667519; this version posted June 11, 2019. The copyright holder for this preprint (which was not certified by peer review) is the author/funder. All rights reserved. No reuse allowed without permission.

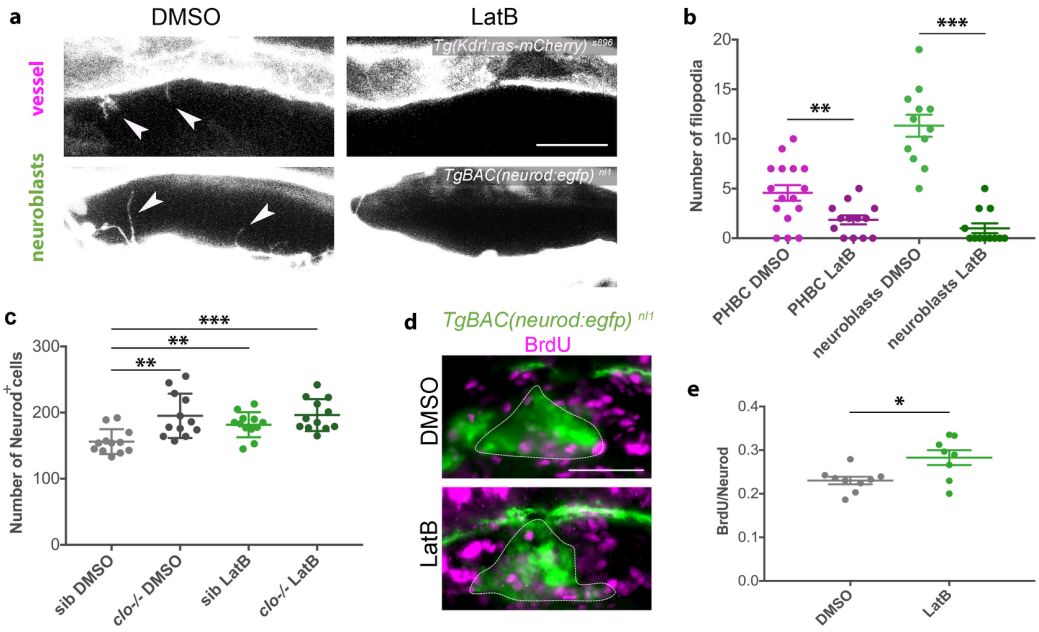

Figure 4. Inhibition of filopodial processes by Latrunculin B results in expansion of neuroblasts.

a, Confocal lateral images showing filopodial processes in vessels and neuroblasts visualized through *TgBAC(neurod:egfp)* ^{nl1} and *(Kdrl:ras-mCherry)* ^{s896} respectively, after 6h treatment in DMSO or LatB, at 30 hpf. Arrowheads indicate filopodia. **b**, Quantification of filopodial processes number in vessels (n = 13-16) and neuroblasts (n = 12) after 6 hours incubation with LatB compared with control (DMSO), at 30 hpf. **c**, Graph showing the number of Neurod^{+} nuclei at 36 hpf, using the *TgBAC(neurod:egfp)* ^{nl1} background and DAPI staining, in sib and clo $^{-/-}$ embryos treated with DMSO or LatB from 24-30 hpf and washed until 36 hpf (n = 12). **d**, Lateral images of BrdU incorporation (magenta) in Neurod^{+} cells of the SAG (dotted line), visualized through *TgBAC(neurod:egfp)* ^{nl1}, in 6 hours DMSO and LatB treated embryos, at 30 hpf. **e**, Graph showing the ratio of BrdU^{+} cells in the Neurod^{+} population after 6 hours DMSO (n = 9) and LatB (n = 8) treated embryos, at 30 hpf.

Scale bars, 20 µm in **a** and 50 µm in **d**. Error bars, mean ± SEM. In **b**,**e** unpaired two-tailed Student's *t*-test was performed. In **c** the data was analyzed using one-way ANOVA, followed by post-hoc test. * $p < 0.05$, ** $p < 0.01$, *** $p < 0.001$. PHBC, primordial hindbrain channel; sib, siblings.

bioRxiv preprint doi: https://doi.org/10.1101/667519; this version posted June 11, 2019. The copyright holder for this preprint (which was not certified by peer review) is the author/funder. All rights reserved. No reuse allowed without permission.

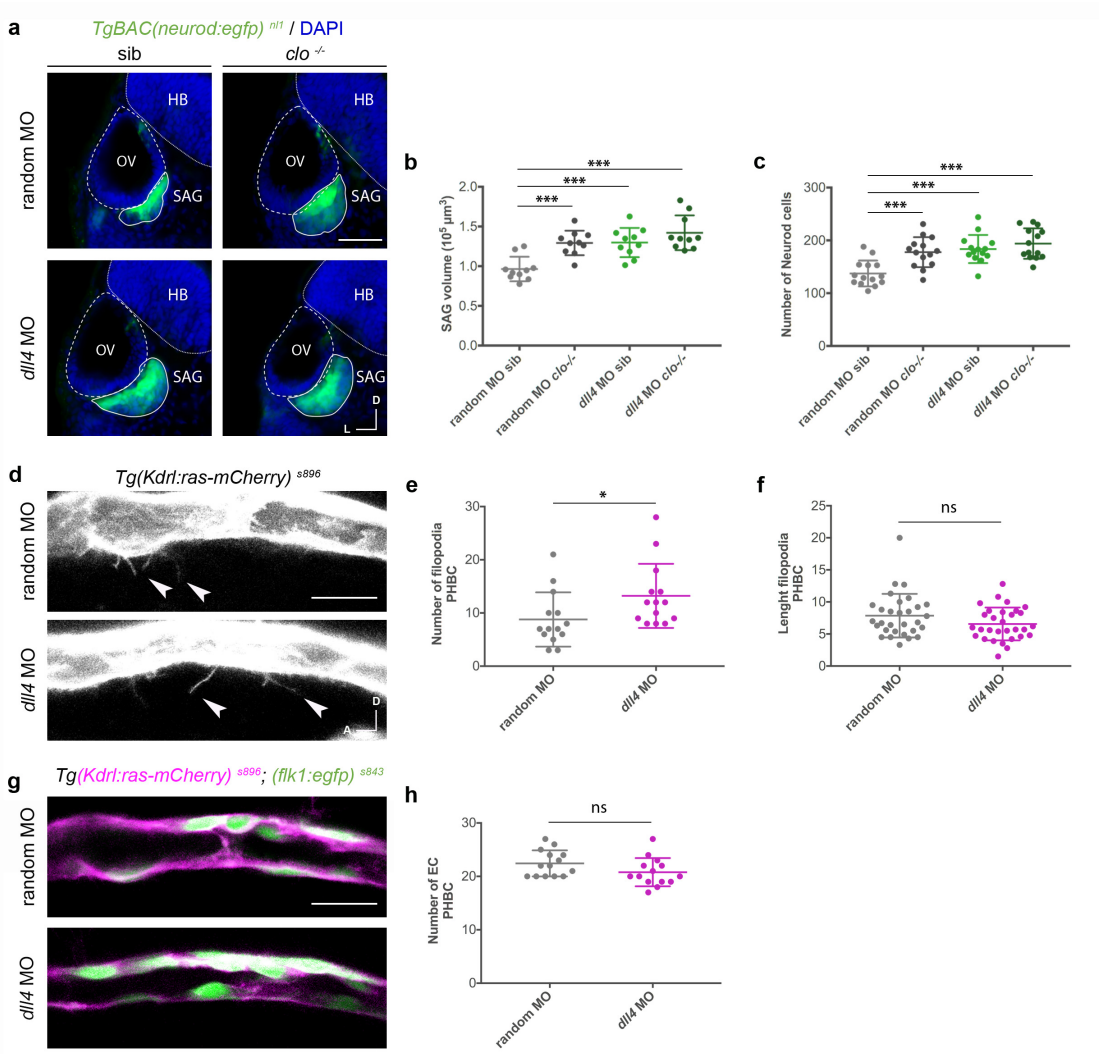

Figure 5. Down-regulation of Dll4 signaling induces neuroblast expansion.

a, Representative transversal images showing the SAG in sib and clo$^{-/-}$ *TgBAC(neurod:egfp)* ^{nl1} embryos injected with of random or *dll4* splicing morpholino. Neurod^{+} cells: green, neuroblasts; DAPI: blue, nuclei. **b**, Graph showing SAG volume quantification in sib and clo$^{-/-}$ embryos injected with random or *dll4* splicing morpholino (n = 10), at 36 hpf. **c**, Graph showing quantification of Neurod^{+} nuclei in sib and clo$^{-/-}$ embryos injected with random or *dll4* splicing morpholino (n = 14), at 36 hpf. **d**, Confocal lateral images of PHBC filopodial processes in random and *dll4* morphants visualized with the *Tg(Kdrl:ras-mCherry)* ^{s896}, at 30 hpf. Arrowheads indicate filopodia. **e**-**f**, Quantification of PHBC filopodia number (n = 14) (**e**) and length (n = 14) (**f**), in random and *dll4* morphants, at 30 hpf. **g**, Confocal lateral images showing EC membranes and cytoplasm using the *Tg(Kdrl:ras-mCherry)* ^{s896} and *Tg(flk1:egfp)* ^{s843} respectively, in the PHBC, at 30 hpf. **h**, Quantification of EC number in random and *dll4* morphants (n = 14), at 30 hpf.

Scale bars, 50 µm in **a**, and 20 µm in **d**,**g**. Error bars, mean ± SEM. In **b**,**c** the data was analyzed using one-way ANOVA, followed by post-hoc test. In **e** the non-parametric Mann-Whitney *U* test was performed. In **f**,**h** unpaired two-tailed Student's *t*-test was used. * $p < 0.05$, ** $p < 0.01$, *** $p < 0.001$. HB, hindbrain; OV, otic vesicle; SAG, statoacoustic ganglion; PHBC, primordial hindbrain channel; EC, endothelial cell.

bioRxiv preprint doi: https://doi.org/10.1101/667519; this version posted June 11, 2019. The copyright holder for this preprint (which was not certified by peer review) is the author/funder. All rights reserved. No reuse allowed without permission.

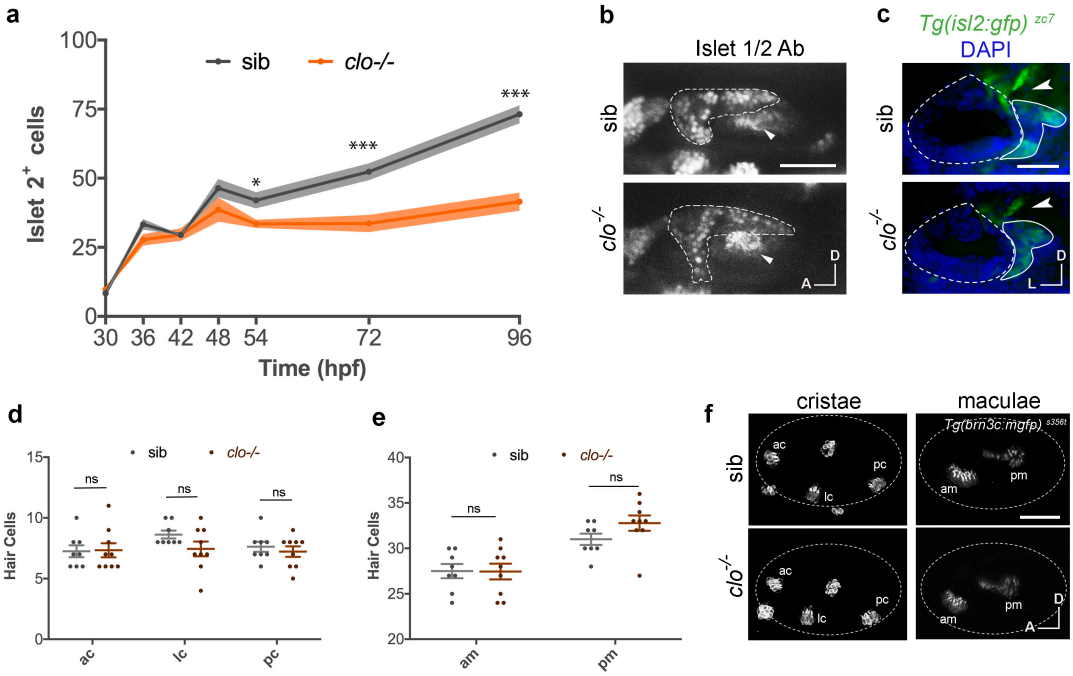

Figure 6. Sensory neuronal differentiation requires blood vessels.

a, Graph showing the number of Islet 2^+ nuclei in the SAG at different timepoints from 30 to 96 hpf (n = 4-10). **b**, Confocal lateral images of immunostained Islet2^+ nuclei in the SAG (dotted line, visualized by *TgBAC(neurod:egfp)* ^{nl1}) in sib and clo$^{-/-}$ embryos at 72 hpf. Arrowheads indicate pm. **c**, Transversal images showing axon density (arrowhead) in the *Tg(isl2:gfp)* ^{zc7} in sib and clo$^{-/-}$ embryos, of cryostat sections, at 72 hpf. Dotted line indicates OV and continuous line the SAG. **d**-**e**, Graph showing quantification of hair cell number in cristae (**d**) and maculae (**e**) in sib (n = 8) and clo$^{-/-}$ (n = 9) embryos. **f**, Representative lateral images of hair cells in cristae and maculae using the *Tg(brn3c:mGFP)* ^{s356t}, at 72 hpf. Dotted line indicates otic vesicle. Non-labelled hair cells are neuromasts.

Scale bars, 50 µm. Error bars, mean ± SD for **a**; and mean ± SEM for **d**,**e**. Unpaired two-tailed Student's *t*-test. * $p < 0.05$, ** $p < 0.01$, *** $p < 0.001$. ns, non-significant. OV, otic vesicle; SAG, statoacoustic ganglion; ac, anterior crista; lc, lateral crista; pc, posterior crista; am, anterior macula; pm, posterior macula; sib, siblings.

bioRxiv preprint doi: https://doi.org/10.1101/667519; this version posted June 11, 2019. The copyright holder for this preprint (which was not certified by peer review) is the author/funder. All rights reserved. No reuse allowed without permission.

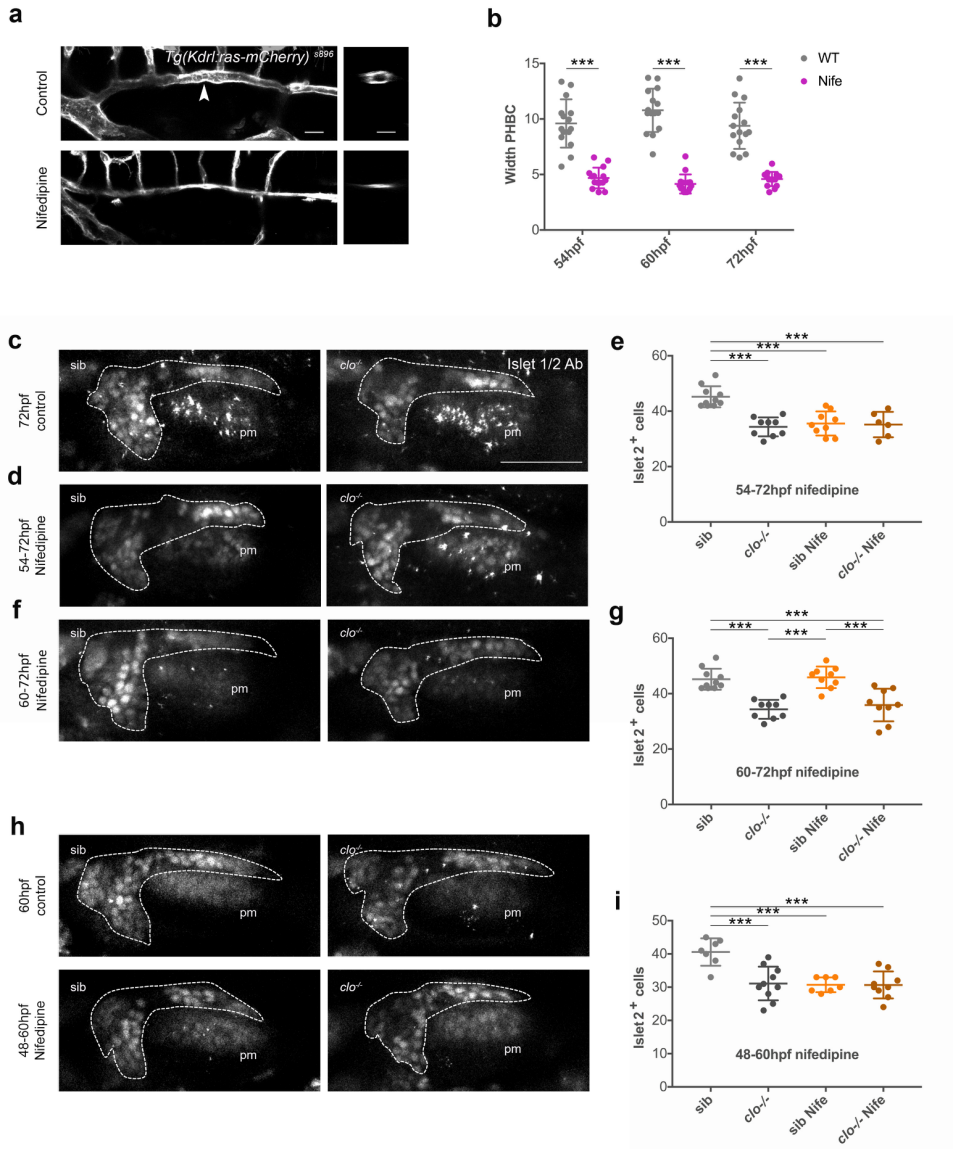

Figure 7. Blood flow is the signal that triggers sensory neuronal differentiation in a restricted temporal window.

a, Representative images of the PHBC of control and 48-54 hpf Nifedipine treated *Tg(Kdrl:ras-mCherry)* ^{s896} embryos, at 54 hpf, in lateral (right) and transversal optic reconstructions (left) in the point marked by the arrowhead. **b**, Analysis of PHBC width in control and Nifedipine treated *Tg(Kdrl:ras-mCherry)* ^{s896} embryos, at 54, 60 and 72 hpf with treatment starting at 48 hpf (n=15). **c,d,f**, Confocal lateral images showing immunostained Islet2^{+} nuclei in the SAG (dotted line, visualized by *Tg(neurod:egfp)* ^{nl1}) in sib and clo$^{-/-}$ embryos at 72 hpf in control (untreated) (**c**), 54-72 hpf Nifedipine treated embryos (**d**), 60-72 hpf Nifedipine treated embryos (**f**), and quantified in **e**,**g**. 72 hpf sib (n = 10), 72 hpf clo$^{-/-}$ (n = 9), 54-72 hpf sib Nife (n = 9), 54-72 clo$^{-/-}$ Nife (n = 6), 60-72 hpf sib Nife (n = 9), 60-72 hpf clo$^{-/-}$ Nife (n = 9). **h**, Confocal images showing immunostained Islet2^{+} nuclei in the SAG (dotted line, visualized by *TgBAC(neurod:egfp)* ^{nl1}) at 60 hpf in control (untreated) and 48-60 hpf Nifedipine treated sib and clo$^{-/-}$ embryos; and quantified in **i**. 60 hpf sib (n = 7), 60 hpf clo$^{-/-}$ (n = 10), 48-60 hpf sib (n = 7), 48-60 hpf clo$^{-/-}$ (n = 9). Scale bars, 50 µm for **a**,**b**,**d**,**f**, and 20 µm for **h**. Error bars, mean ± SEM. Unpaired two-tailed Student's *t*-test. * $p < 0.05$, ** $p < 0.01$, *** $p < 0.001$. ns, non-significant. pm, posterior macula; Nife, Nifedipine; sib, siblings; PHBC, primordial hindbrain channel.

bioRxiv preprint doi: https://doi.org/10.1101/667519; this version posted June 11, 2019. The copyright holder for this preprint (which was not certified by peer review) is the author/funder. All rights reserved. No reuse allowed without permission.

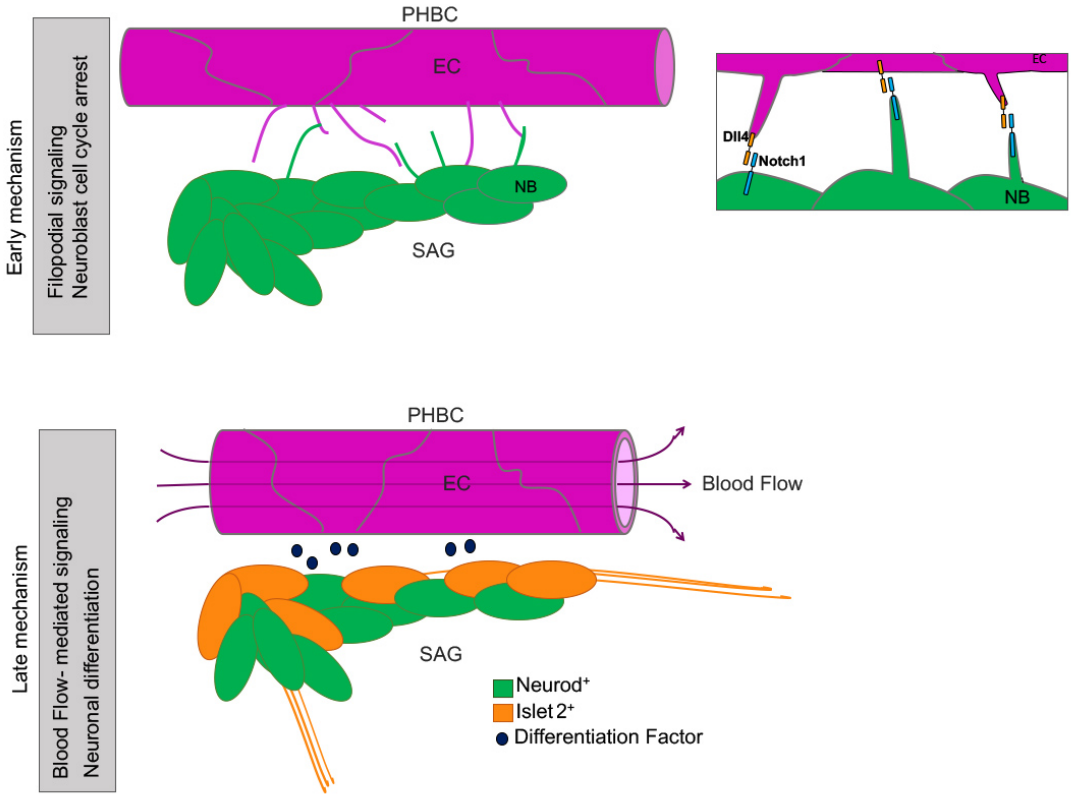

Figure 8. Proposed mechanism model.
EC regulate NB behaviour by two independent and temporally separated mechanisms. At early stages, filopodial processes from both EC and NB contact each other. These contacts allow dll4-notch1 signalling that reduces the cycling of the NB. At late stages, blood flow onset triggers NB terminal differentiation into neurons. EC, endothelial cell; NB, neuroblast; PHBC, primordial hindbrain channel; SAG, statoacoustic ganglion.

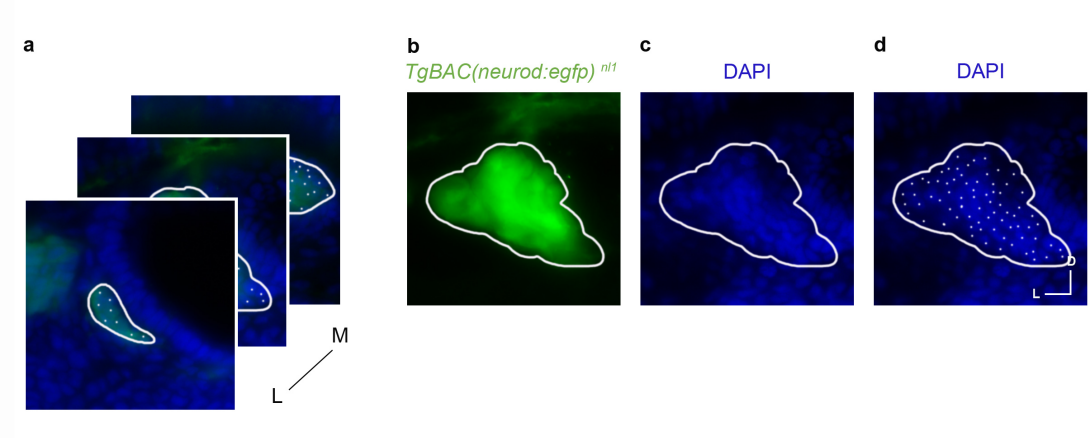

Supplementary Figure 1. Protocol used for quantification of Neurod+ cell number.
a-**d**, For a series of latero-medial in sagittal or antero-posterior transversal (data not shown) cryostat sections, the perimeter of the SAG was drawn using the green signal of *TgBAC(neurod:egfp)* ^{nl1} (**b**), subsequently green light was hidden and blue light from DAPI staining was visualized (**c**) to manually count the number of cells (**d**).

bioRxiv preprint doi: https://doi.org/10.1101/667519; this version posted June 11, 2019. The copyright holder for this preprint (which was not certified by peer review) is the author/funder. All rights reserved. No reuse allowed without permission.

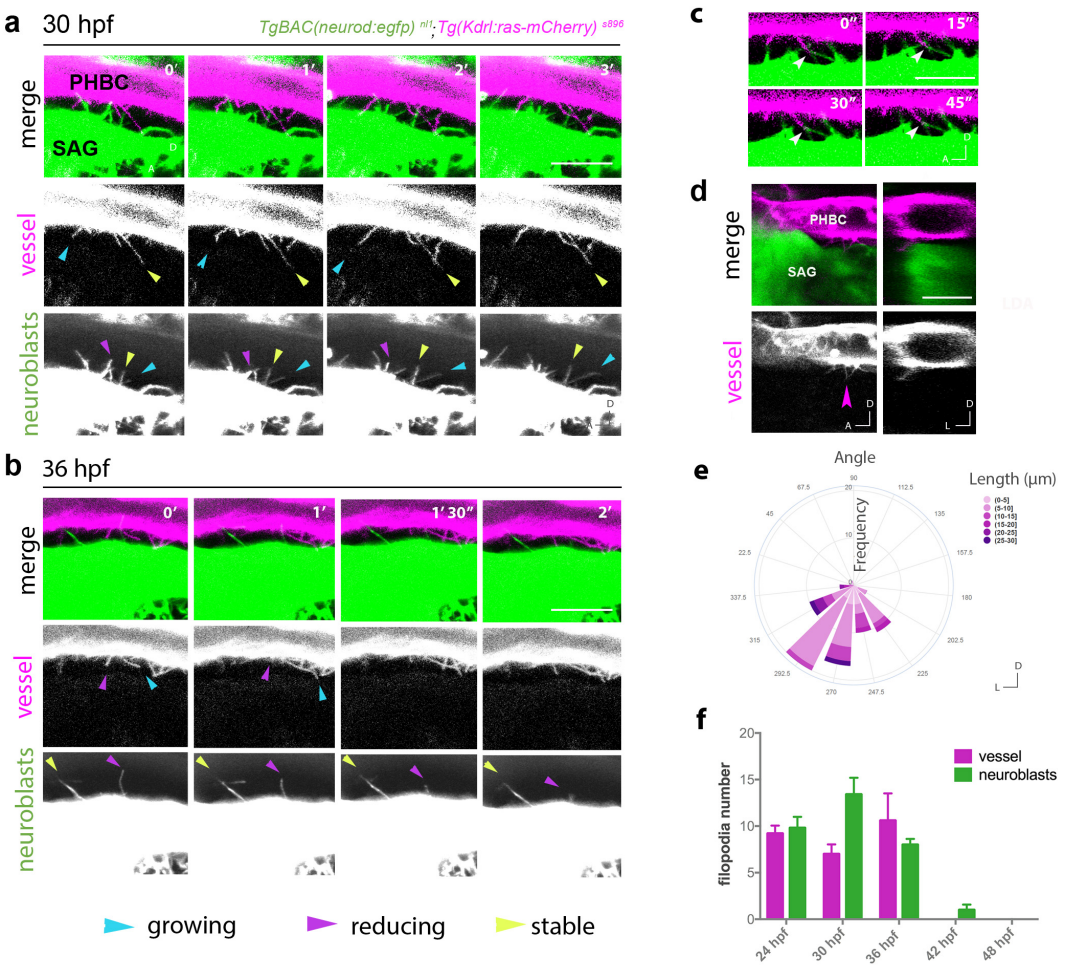

Supplementary Figure 2. EC from the PHBC and neuroblasts from the SAG extend filopodia towards each other from 24 to 36 hpf.

a-**c**, Still images of time-lapse videos of *TgBAC(neurod:egfp)*^{nl1}*; (Kdrl:ras-mCherry)*^{s896} showing filopodia extending from the PHBC to neuroblasts and from neuroblasts to PHBC at 24 hpf (**a**), 30 hpf (**b**), and 36 hpf (**c**) (time-lapses are representative of 5 experiments), in a lateral view. Cyan, magenta and yellow arrowheads point to examples of growing, reducing and stable filopodia, respectively. Scale bar 50 µm. PHBC, primordial hindbrain channel.

bioRxiv preprint doi: https://doi.org/10.1101/667519; this version posted June 11, 2019. The copyright holder for this preprint (which was not certified by peer review) is the author/funder. All rights reserved. No reuse allowed without permission.

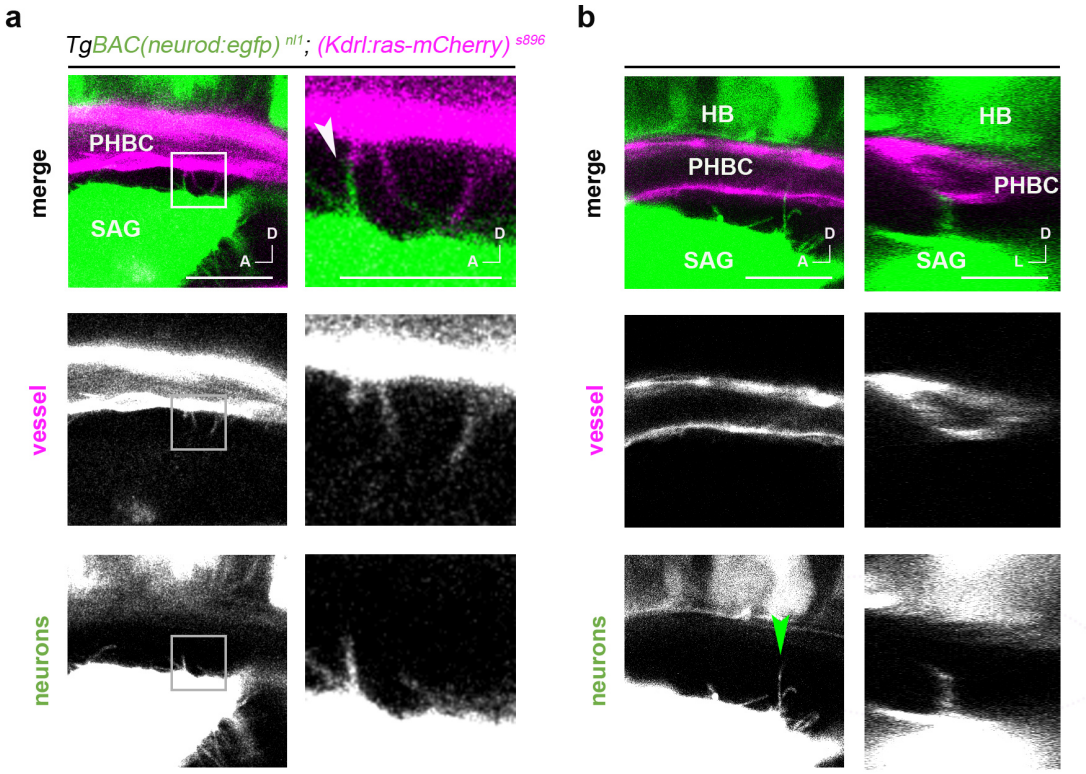

Supplementary Figure 3. Filopodia from vasculature and neuroblasts contact each other at the same plane.

a, Confocal lateral image of a single plane showing a filopodia-filopodia contact between EC and neuroblasts. Square shows magnified image in the right, and arrowhead the mentioned contact. **b**, Confocal lateral image of a single plane and transverse optical reconstruction also in single plane showing a filopodial process from the neuroblasts contacting the EC. Arrowhead indicates point for transverse optical reconstruction. Scale bar 20 µm. PHBC, primordial hindbrain channel; SAG, statoacoustic ganglion; HB, hindbrain.

bioRxiv preprint doi: https://doi.org/10.1101/667519; this version posted June 11, 2019. The copyright holder for this preprint (which was not certified by peer review) is the author/funder. All rights reserved. No reuse allowed without permission.

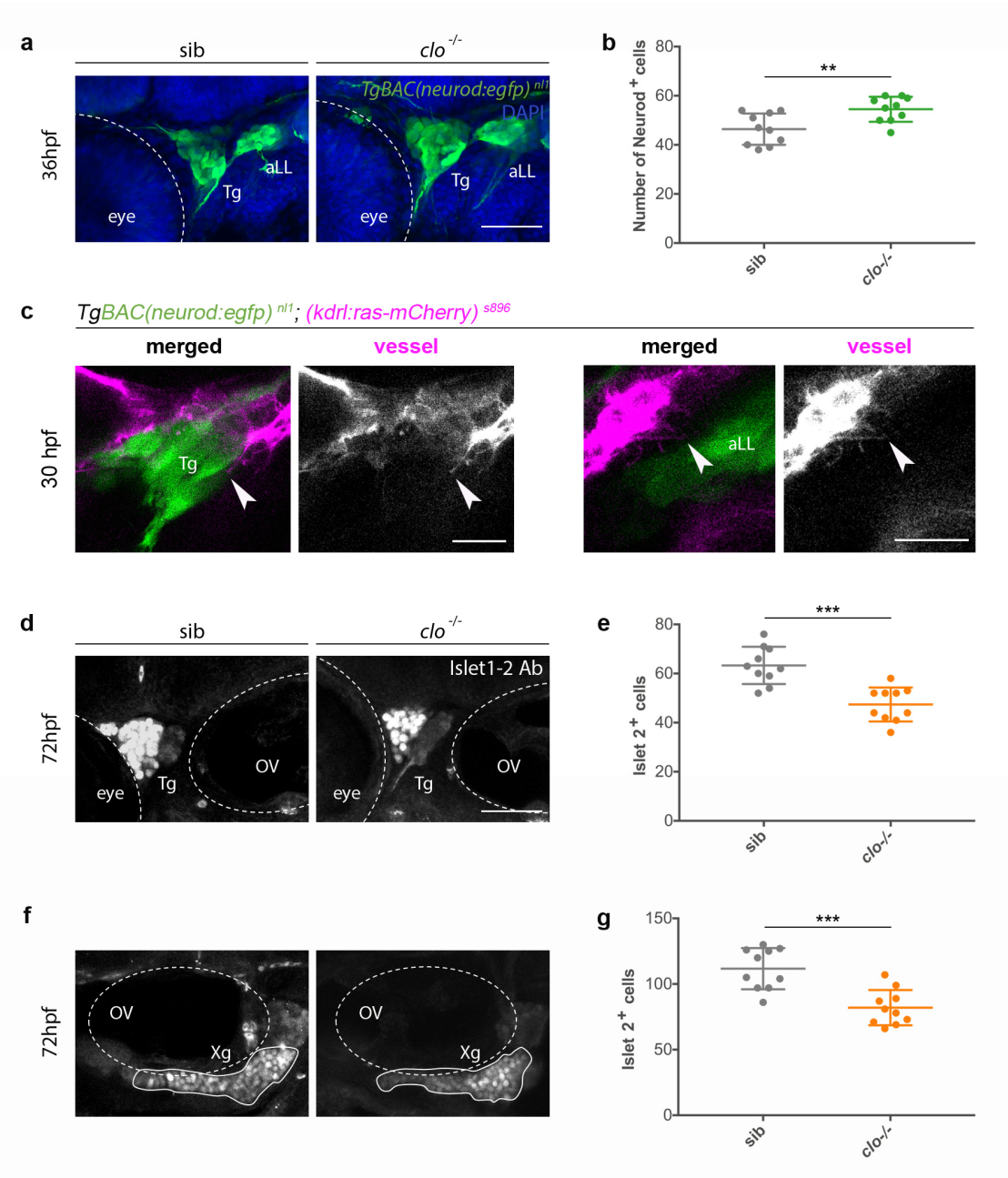

Supplementary Figure 4. Filopodial contacts and defects on sensory neurogenesis in absence of vasculature in other sensory ganglia.

a, Confocal lateral images of Tg and aLL ganglia in sib and clo$^{-/-}$ *TgBAC(neurod:egfp)^{nl1}* embryos, at 36 hpf. Neurod^{+} cells: green, neuroblasts; DAPI: blue, nuclei. **b**, Quantification of Neurod^{+} cells in the Tg of sib and clo$^{-/-}$ embryos, at 36 hpf (n = 10). **c**, Confocal lateral images of a single plane showing filopodial processes from the PHBC contacting neuroblasts of the Tg and aLL ganglia. Arrowheads indicate filopodia. **d**-**g**, Confocal lateral images showing the number of Islet2^{+} nuclei in the Tg (**c**) and Xg ganglia (**e**) through Islet 1/2 antibody staining and quantified in **e** and **g** respectively (n = 10), at 72 hpf.

Scale bars 50 µm for **a**, **b**, **d**-**g**, and 20 µm for **c**. Error bars, mean ± SEM. Unpaired two-tailed Student's *t*-test. * $p < 0.05$, ** $p < 0.01$, *** $p < 0.001$. ns, non-significant. Tg, Trigeminal ganglion; aLL, anterior Lateral Line, OV, Otic Vesicle; Xg, Vagus ganglion; sib, siblings.

bioRxiv preprint doi: https://doi.org/10.1101/667519; this version posted June 11, 2019. The copyright holder for this preprint (which was not certified by peer review) is the author/funder. All rights reserved. No reuse allowed without permission.

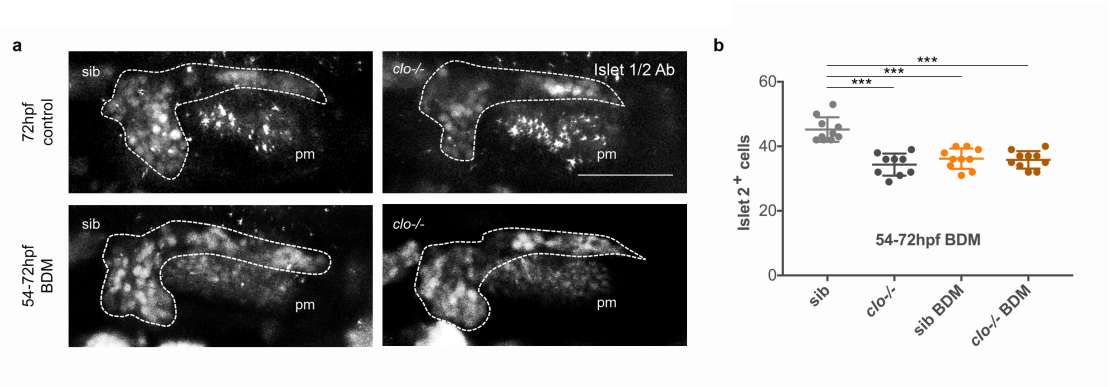

Supplementary Figure 5. Blood flow arrest by BDM also prevents Islet2^{+} neuronal differentiation.

a, Confocal lateral images showing immunostained Islet2^{+} nuclei in the SAG (dotted line, visualized by *TgBAC(neurod:egfp)* ^{nl1}) in sib and clo$^{-/-}$ embryos at 72 hpf in control (untreated) and 54-72 hpf BDM treated embryos. **b**, Graph showing the number of Islet 1/2^{+} cells in sib (n = 10), clo$^{-/-}$ (n = 9), 54-72 hpf sib BDM (n = 10), and 54-72 hpf clo$^{-/-}$ BDM (n = 10). Scale bar 50 µm. Error bars mean ± SEM. Unpaired two-tailed Student's *t*-test. * $p < 0.05$, ** $p < 0.01$, *** $p < 0.001$. ns, non-significant. pm, posterior macula; sib, siblings.

Number of neurod^{+} cells in the SAG

hpf	30	36	42	48	54	72
E1	77	132	143	109	100	103
E2	81	146	125	108	93	90
E3	105	144	138	100	99	120
E4	107	124	136	131	130	78
E5	105	139	109	145	128	132
E6	110	141	113	111	165	106
E7	92	140	125		148	
E8	75	103	116		109	
E9	115	102			108	
E10	101	108			118	
count	10	10	8	6	10	6
Prom	88,43	127,90	125,63	117,33	119,80	104,83
SD	14,54	17,47	12,49	17,03	23,12	19,56
SEM	4,60	5,52	4,42	6,95	7,31	7,99

Number of Islet 2^{+} cells in the SAG

hpf	30	36	42	48	54	72	96
E1	10	33	28	40	46	56	88
E2	7	40	31	41	62	54	66
E3	11	41	28	58	37	48	75
E4	9	42	31	47	39	40	76
E5	7	29		46	45	56	74
E6	5	31			40	60	62
E7	9	27			40		71
E8	9	27			35		
E9		31			34		
E10		32					
count	8	10	4	5	9	6	7
Prom	8,38	33,30	29,50	46,40	42,00	52,33	73,14
SD	1,92	5,68	1,73	7,16	8,51	7,20	8,30
SEM	0,68	1,80	0,87	3,20	2,84	2,94	3,14

Supplementary Table 1. Number of Neurod^{+} and Islet2^{+} cells from 30 to 96 hpf.

Tables showing the number of quantified cells per embryo of the Neurod^{+} cell population and Islet2^{+} cell population. Neurod^{+} cells were quantified using the *TgBAC(neurod:egfp)* ^{nl1} and DAPI staining. Islet 2^{+} cells were quantified using immunostaing with Islet 1-2 antibody, which is nuclear.

bioRxiv preprint doi: https://doi.org/10.1101/667519; this version posted June 11, 2019. The copyright holder for this preprint (which was not certified by peer review) is the author/funder. All rights reserved. No reuse allowed without permission.

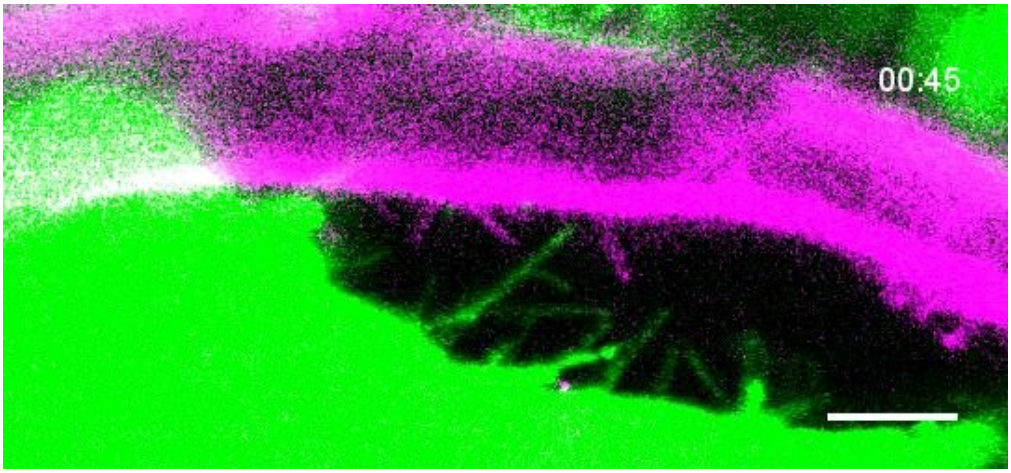

Supplementary Video 1. Filopodial processes of the endothelial cells and neuroblasts contact each other at 30 hpf.
Z-projection time-lapse video of *TgBAC(neurod:egfp)*^{nl1}*; (Kdrl:ras-mCherry)*^{s896} embryos showing filopodia extending from the PHBC to the SAG and from the SAG to the PHBC at 30 hpf. Note thickenings in some neuroblasts filopodial. Lateral view. Scale bar 10 µm.

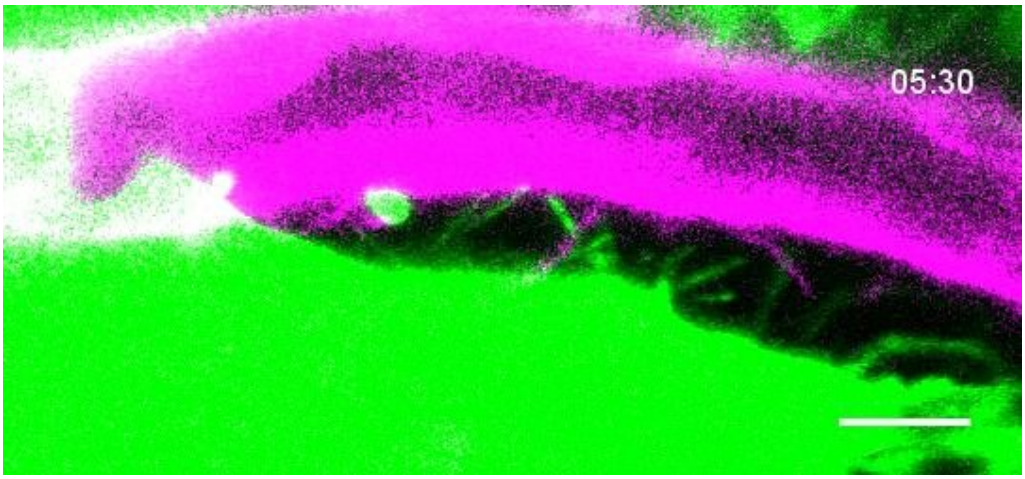

Supplementary Video 2. Filopodial processes of the endothelial cells and neuroblasts contact each other at 30 hpf.
Z-projection time-lapse video of *TgBAC(neurod:egfp)*^{nl1}*; (Kdrl:ras-mCherry)*^{s896} embryos showing filopodia extending from the PHBC to the SAG and from the SAG to the PHBC at 30 hpf. Note dynamism of filopodial processes. Lateral view. Scale bar 10 µm.

bioRxiv preprint doi: https://doi.org/10.1101/667519; this version posted June 11, 2019. The copyright holder for this preprint (which was not certified by peer review) is the author/funder. All rights reserved. No reuse allowed without permission.

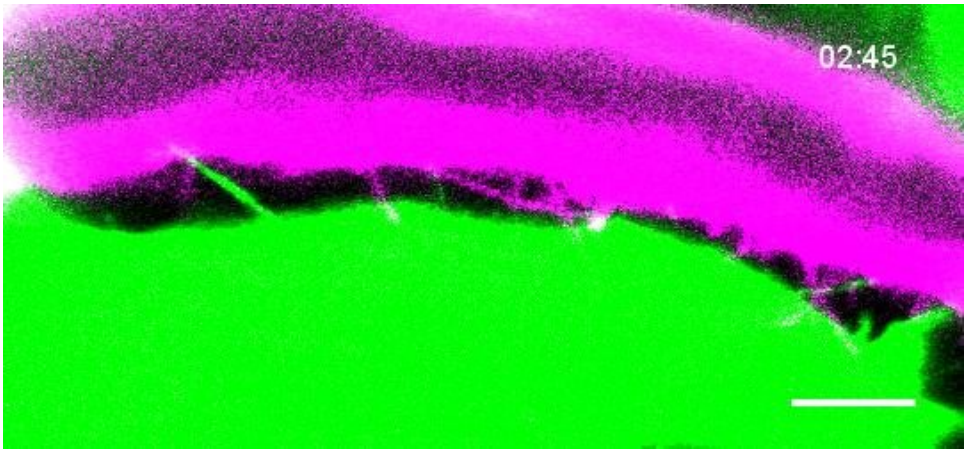

Supplementary Video 3. Filopodial processes of the endothelial cells and neuroblasts contact each other at 36 hpf.
Z-projection time-lapse video of *TgBAC(neurod:egfp)*^{nl1}*; (Kdrl:ras-mCherry)*^{s896} embryos showing filopodia extending from the PHBC to the SAG and from the SAG to the PHBC at 36 hpf. Note dynamism of filopodial processes. Lateral view. Scale bar 10 µm.

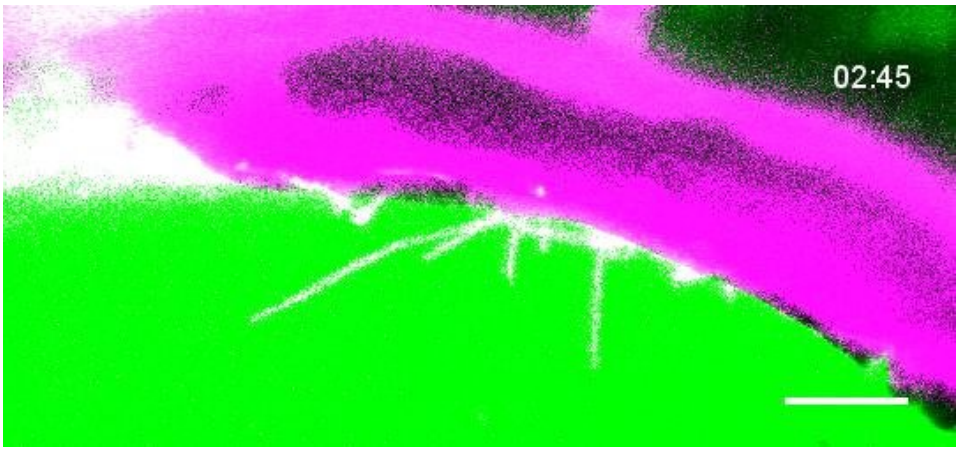

Supplementary Video 4. Filopodial processes of the endothelial cells and neuroblasts contact each other at 36 hpf.
Z-projection time-lapse video of *TgBAC(neurod:egfp)*^{nl1}*; (Kdrl:ras-mCherry)*^{s896} embryos showing filopodia extending from the PHBC to the SAG and from the SAG to the PHBC at 36 hpf. Note length of EC filopodia. Lateral view. Scale bar 10 µm.